CHAPTER 8 TRIAXIAL TEST DATA AND RESULTS

Introduction

Consolidated undrained (CU) triaxial compression tests were performed on three different sands in order to characterize the steady state relationship for each, which relates void ratio and steady state undrained shear strength for a particular material. Since no ASTM standard test method exists for CU triaxial tests on granular materials, the procedures for test preparation outlined in Chapter 3, which are based on Head (1986), were followed. Two series of tests were performed on each material: one with conventional end platens with sintered bronze drainage inserts, and one with lubricated end platens. The three materials, Light Castle sand, Monterey #0/30 sand, and Ottawa sand, are all classified as poorly graded sands (SP) according to the Unified Soil Classification System (USCS), which is outlined in *ASTM D 2487-93* (ASTM 1995). The properties of the three sands are given in Appendix E. Each of the materials contains less than 1 percent fines (material passing the #200 sieve) and all three possess fairly uniform grain size distributions, as shown in Figure 8.1. The maximum and minimum index densities determined according to *ASTM D4253-91* and *ASTM D4254-91* (ASTM 1995), maximum and minimum void ratios, and specific gravity determined according to *ASTM D854-92* (ASTM 1995) for each material are shown in Table 8.1.

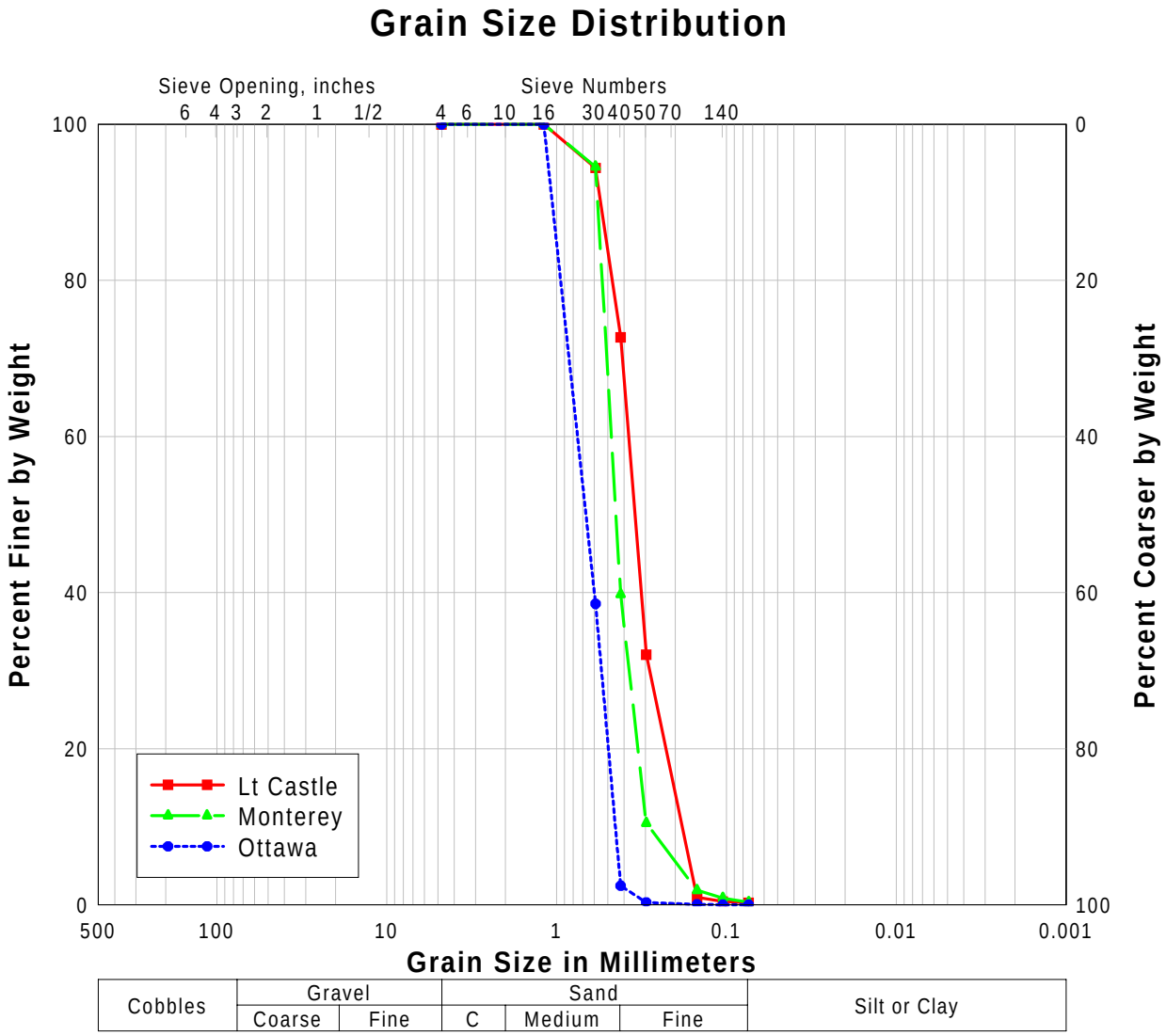

Figure 8.1 - Grain Size Distributions for the Test Materials

Table 8.1 - Index Density, Index Void Ratio, and Specific Gravity

	Light Castle	Monterey	Ottawa
G_s	2.65	2.65	2.65
γ_{dmax} (pcf)	108.2	107.4	112.0
γ_{dmin} (pcf)	91.4	91.0	95.0
e_{min}	0.528	0.540	0.476
e_{max}	0.809	0.817	0.741

Light Castle sand is composed of subangular quartz grains, and was obtained from a quarry in Craig County Virginia (Filz 1992). Monterey #0/30 sand is composed primarily of subrounded to subangular quartz grains (Sehn 1990). Ottawa sand consists of rounded quartz grains and is obtained from the Ottawa Silica Company in Illinois.

The diameter of all triaxial test specimens was 2.8 inches and the ratio of length to diameter (L/D) was approximately 2.1. The height of the specimens tested using conventional end platens was 6.0 inches, and the height of the specimens tested using lubricated end platens was 5.85 inches. The specimens were encapsulated by a latex rubber membrane that was 0.012 inches thick. A hydraulic piston with flow control valves to ensure a constant rate of axial displacement applied the axial load. The axial load was measured using a conventional load cell, and pore pressure was measured using a differential pressure transducer. Several load-controlled tests were performed, but the majority of the tests conducted in the course of this research were strain-controlled. Strain-controlled tests are more common than load-controlled tests in most laboratories and they are preferred for determination of steady state properties in the triaxial test (Poulos et al. 1985). For the strain-controlled tests, an axial displacement was applied at a constant rate, and the resulting

axial force and change in pore pressure (effective stress) were measured. Since all three of the sands tested contained little or no fines, the permeabilities and consolidation rates for each were very high. As a result, the strain rate for the shear phase of all tests was not determined based on consolidation properties. Instead, the maximum strain rate suggested by Head (1986) for CU tests, which is 0.1 percent per minute, was used for all strain-controlled tests. Two series of tests were performed on each material: one using conventional end platens with sintered bronze drainage inserts, and one using lubricated end platens.

Lubricated End Platens

For the lubricated end platen tests, oversized end platens 3.4 inches in diameter were fabricated in order to accommodate radial expansion of the specimen at the end platen while ensuring that the ends of the specimen remain plane. Modifications were also made to the drainage scheme for the oversized platens. A photograph of the top platen with the lubrication layers applied is shown in Figure 8.2. The bottom platen, with only one lubrication layer applied is shown in Figure 8.3. The sintered bronze or porous stone drainage inserts in conventional triaxial test end platens can transmit significant shear stresses to the specimen, and covering the drainage insert with lubrication material would impede the flow of pore water into or out of the insert. For clean sandy materials such as those used in this study, the permeability is typically high enough so that adequate drainage can be provide by a much smaller drainage element in the end platen. The oversized platens were designed to allow the use of a small drainage line (0.125-inch diameter tubing) located concentrically in the platen in order to facilitate drainage and pore pressure measurement while maximizing the portion of the specimen-platen interface that could be lubricated.

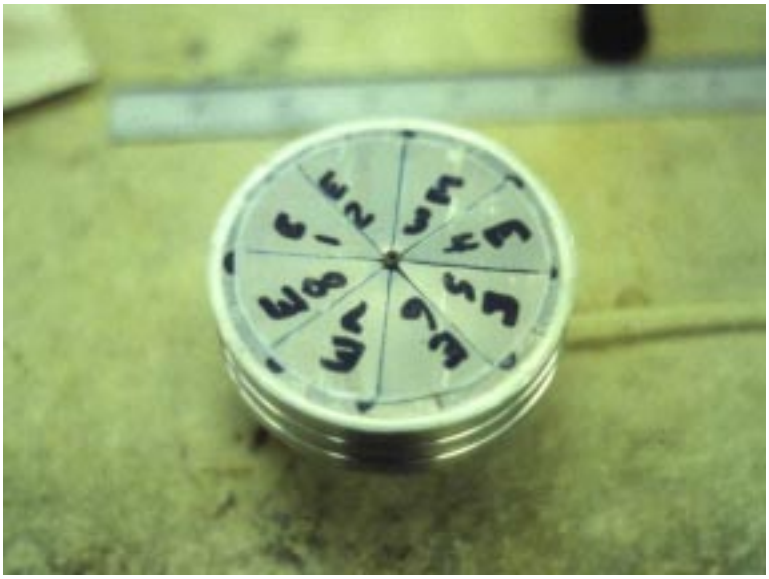

Figure 8.2 – Top Platen with Lubrication Applied

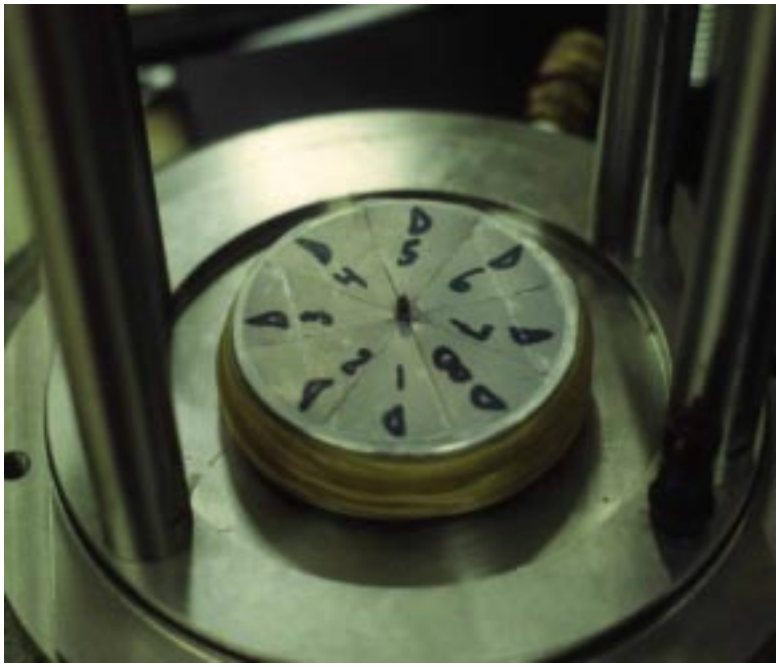

Figure 8.3 – Bottom Platen with Lubrication Applied

Initially, the drainage lines were mounted so that they protruded from the end platen just enough to ensure that the lubrication materials would not clog the

line (about 0.05 inches). Due to the efficiency of the lubricated platens, in this configuration the specimen could slide out from between the end platens if the axial load was not perfectly concentric, the end platens were not perfectly parallel, or the shear resistance did not develop uniformly in the soil. This large unidirectional displacement of the specimen was observed in at least one test, as shown in Figure 8.4 and Figure 8.5. The axis of the specimen migrated to the edge of the end platens in a very short period of time. While load eccentricity on the order of the radius of the specimen severely alters the desired stress state in the specimen and makes data interpretation nearly impossible, this test did provide a convincing demonstration of the efficiency of the lubrication scheme. Consequently, the drainage lines were modified so that they protruded 0.125 inches from the end platen in order to provide resistance to such large unidirectional displacement of the specimen. Lee and Seed (1964) and Lee (1978) used a similar approach to achieve the same effect. Although the presence of the drainage line in the end of the specimen might be expected to increase the shear resistance somewhat, this effect was considered to be negligible since the overall size of the specimen was still quite large when compared to the drainage lines.

Figure 8.4 – Large Unidirectional Displacement of Specimen with Lubricated Ends

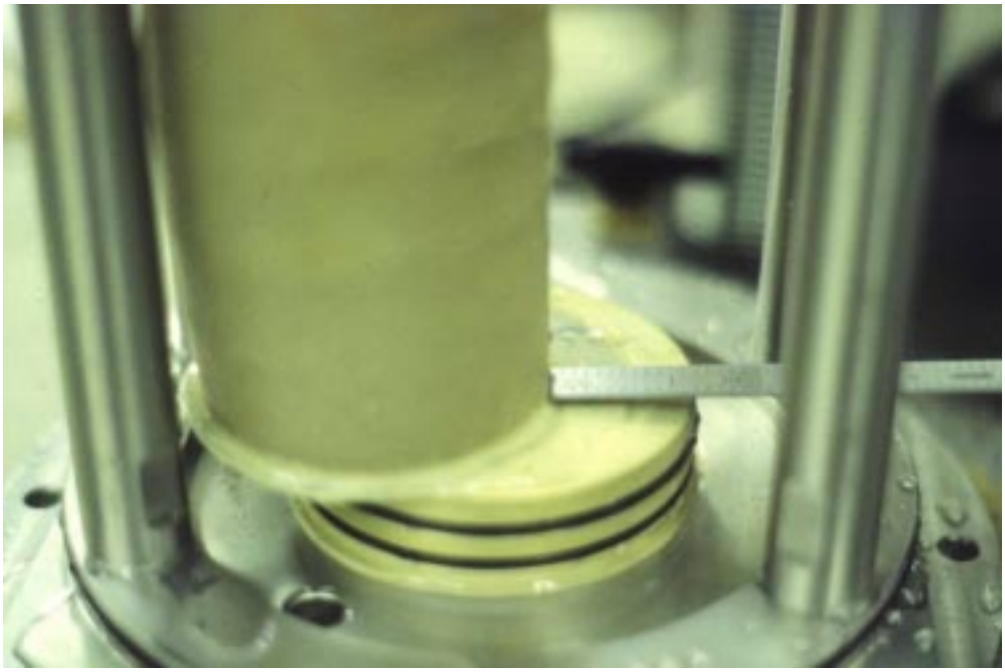

Figure 8.5 – Unidirectional Displacement at Bottom Platen

Two of the lubrication schemes described in Chapter 6 were used in the lubricated end platen tests. The first employed two layers of latex dental dam 0.008 inches thick with a thin layer of Dow Corning high vacuum grease between the two layers of latex and between the latex and the aluminum end platen as shown in Figure 8.6. Different variations of the basic latex-grease lubricated end are the most commonly used for triaxial tests on soft clays (Whitman et al. 1960, Olson and Campbell 1964, Barden and McDermott 1965, Duncan and Dunlop 1968), and have also been used for tests on sands (Rowe and Barden 1964, Tatsuoka et al. 1984, Goto et al. 1993).

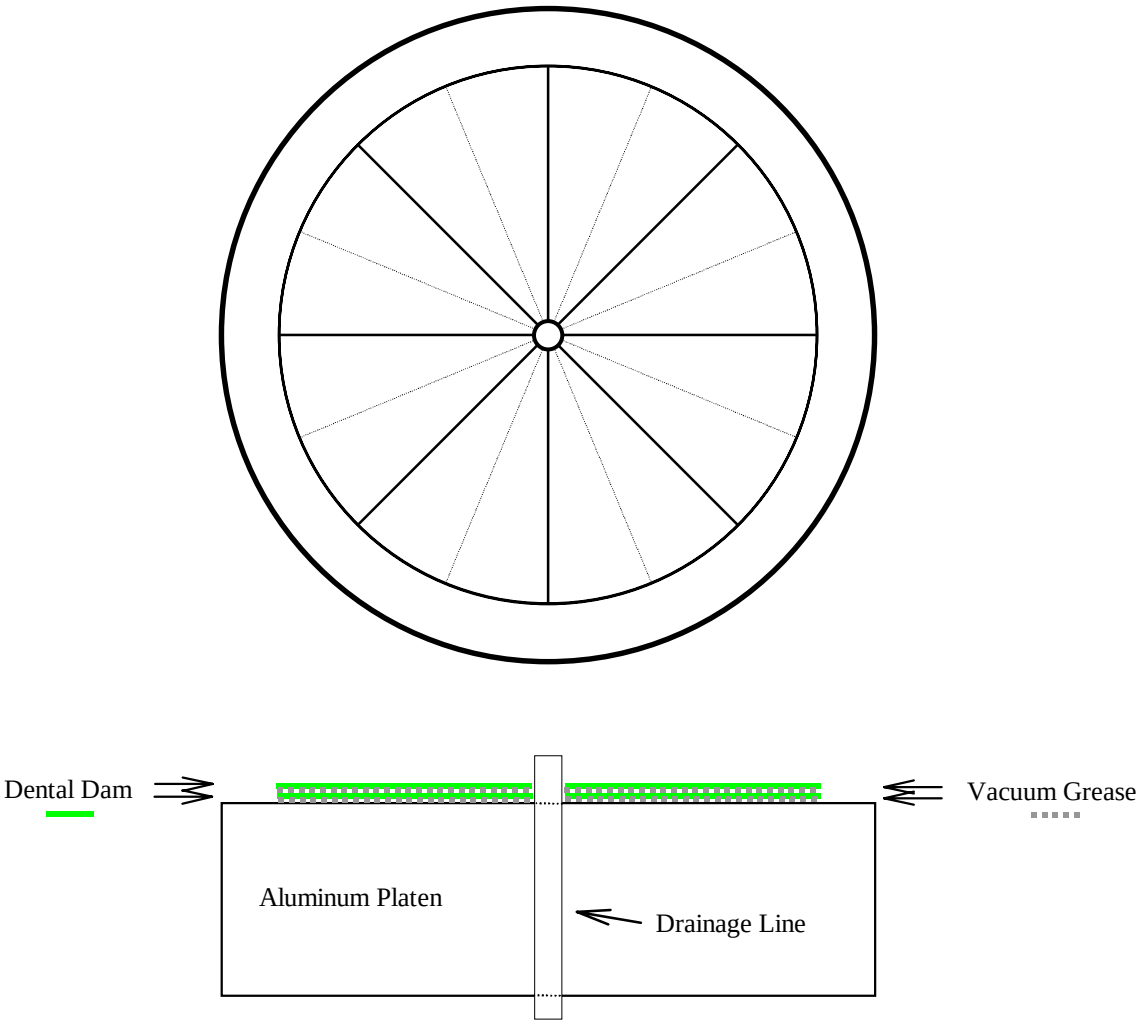

Figure 8.6 - Lubricated End Platen Using Latex Dental Dam and Vacuum Grease

The latex disks were cut into eight equal arc sectors, or *pie* pieces, so that circumferential tension would not develop throughout the entire disk. The radial joints in one layer were offset from those in the other layer to minimize the potential for the grease to migrate into the sand specimen and to minimize the potential for individual sand particles to penetrate between the *pie* pieces. The latex-grease scheme was employed in the lubricated end tests on Ottawa Sand.

When testing granular materials with lubricated ends, friction can develop between individual grains and the end platen due to stress concentrations at the particle contacts. Since the latex is relatively flexible, the stresses between individual grains and the end platen can become quite high and cause compression of the latex and displacement of the grease on a local scale. The second type of lubrication scheme, shown in Figure 8.7, was designed to prevent these stress concentrations on the end platen by providing additional rigidity perpendicular to the interface. Metal shim stock 0.003 inches thick was cut into circular disks like the latex dental dam in the first lubrication scheme. The shim was covered on both sides with poly-tetra-fluoro-ethylene (PTFE, or Teflon) tape that was 0.005 inches thick. The composite disk was then cut into eight sectors and placed in an offset manner like the latex in the latex-grease scheme. The layer of PTFE shim next to the soil specimen was 2.8 inches in diameter, and the layer next to the platen was 3.1 inches in diameter so that as lateral expansion occurred, the double-layer interface would still exist. A thin layer of vacuum grease was placed between the PTFE shim layer and the end platen as well as between the two shim layers. This scheme, using only one layer, performed well in the interface direct shear tests described in Chapter 6, with an interface friction angle less than 1 degree. Even without the layers of vacuum grease, the friction characteristics were comparable to the latex-grease scheme. The lubricated end tests on Light Castle Sand and Monterey Sand were performed using the PTFE shim-grease lubrication scheme.

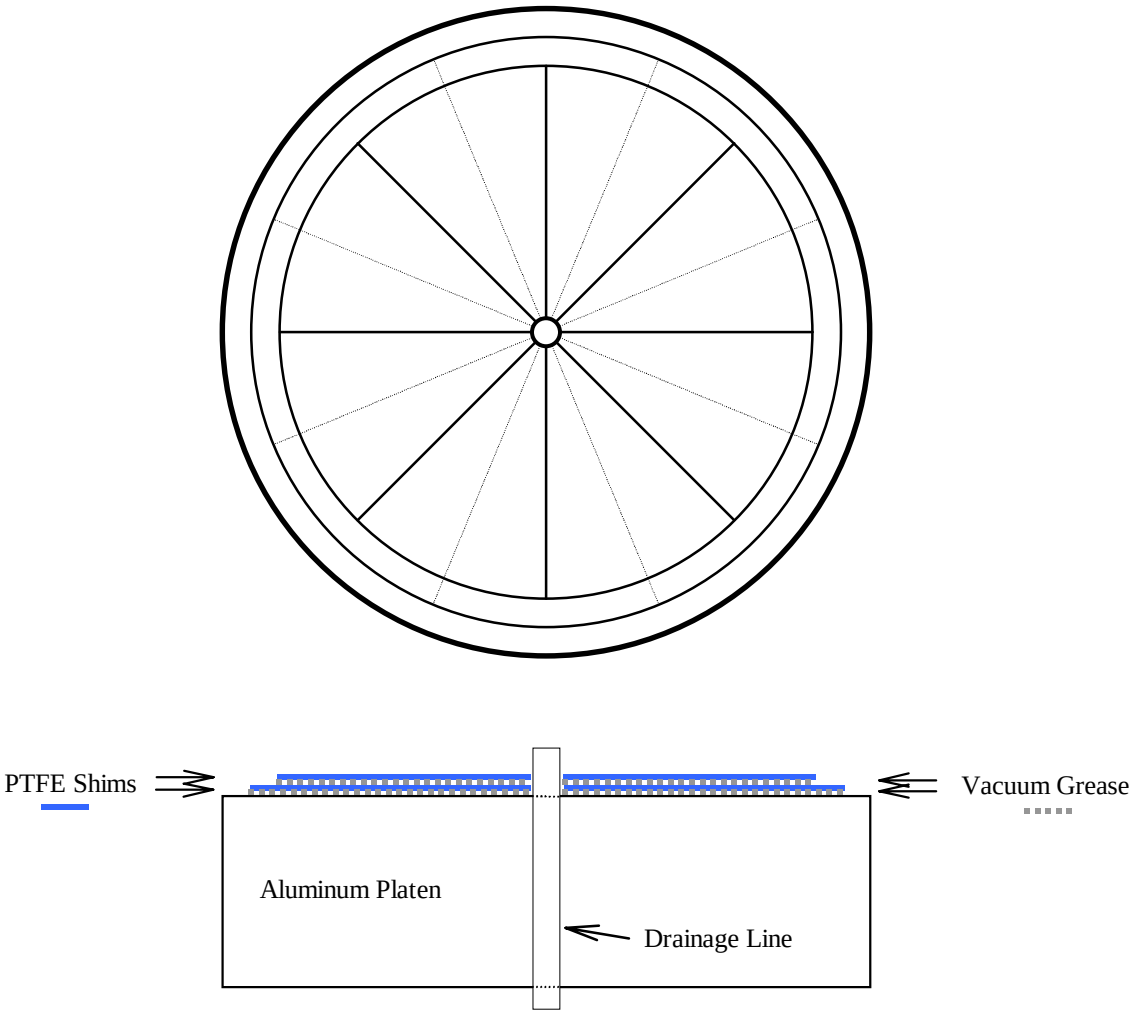

Figure 8.7 - Lubricated End Platen Using PTFE Shims and Vacuum Grease

Specimen Preparation Techniques

Since loose, contractive specimens were desired, a specimen preparation technique that could be used to achieve uniform specimens over a wide range of densities, including very loose, was selected. Dry pluviation techniques, in which the sand is poured through disks or sieves with various opening sizes into the specimen mold, were investigated. Pouring dry sand through a tube in a similar manner to that used in the minimum index density test described by

ASTM D 4254-91 (ASTM 1995), and moist compaction techniques were also evaluated. Moist compaction entails mixing the sand to a water content that facilitates bulking of the sand grains and compacting the specimen in lifts, with precise measurement of the weight of soil and the height for each lift.

For uniform sands, specimens prepared by pluviation in either air or water are somewhat more uniform than those prepared by moist compaction (Castro 1969, Mulilis et al. 1977, Castro et al. 1982, Vaid and Negussey 1988). The major factor influencing the density of pluviated specimens is the porosity of the shutter, which controls the deposition intensity (Eid 1987, Rad and Tumay 1987). As a result, Rad and Tumay (1987) suggested that all factors be kept constant except for the shutter porosity to achieve different relative densities. Vaid and Negussey (1988) indicated that drop height has the most impact on relative density for pluviation in air, and that variation in the drop height should be used to vary the relative density for different specimens. For pluviation under water, Vaid and Negussey (1988) showed that changing the drop height did not significantly change the relative density achieved, and attributed this phenomenon to the fact that the terminal velocity of the particles is reached much more quickly in air than in water. They further showed that if specimens pluviated under water are vibrated to achieve greater densities, the test results will generally agree with those of specimens of the same relative density that were pluviated in air. Although uniform specimens can be achieved over a wide range of relative densities using dry pluviation techniques, it is extremely difficult to produce very loose specimens. The lowest relative density achieved by Vaid and Negussey (1988) for Ottawa Sand, and the lowest relative density achieved by Rad and Tumay (1987) for Monterey Sand was approximately 12 percent. Regardless of the method used to control relative density, very strict tolerance on the control would be required in order to obtain very loose specimens. For example, if using drop height to control density, a very precise drop height would have to be maintained. Furthermore,

the drop height would be very small, and the sensitivity of relative density to drop height increases as drop height decreases, so the desired uniformity is sacrificed when attempting to produce very loose specimens using pluviation techniques (Vaid and Negussey 1988).

In order to determine the range of densities that could be achieved using dry pluviation for the three sands in this study, specimens were prepared using various shutter disks and drop heights, with the intent of producing loose and very loose specimens. The ranges of relative densities achieved are shown in Table 8.2. Since very loose specimens could be prepared only by the pouring method for one of the three sands, an alternative to dry pluviation as a means of specimen preparation for this study was investigated.

Table 8.2 - Specimen Densities Achieved By Dry Pluviation

Material	Range of Relative Densities (%)	
	Dry Pluviation	Pouring
Light Castle Sand	46 to 67	0 to 6
Monterey Sand	66 to 90	21 to 30
Ottawa Sand	82 to 87	43 to 49

Since very loose specimens are desired for determination of steady state using triaxial tests (Poulos et al. 1985), moist compaction, or moist tamping techniques were employed. The moist compaction technique provided relatively uniform specimens, and could be used to prepare specimens with a considerable range of densities, including very loose states with relative densities less than 0 percent. The sand was mixed to a water content of 5 percent to 7 percent and compacted in individually weighed and measured lifts

of one half inch or one inch to control specimen uniformity and void ratio. A special device, similar to that used by Ladd (1978), was constructed in order to facilitate very accurate control of lift height when compacting the specimen. The device consists of a rod and tamper that move vertically through a bushing and sleeve that are attached to the triaxial cell. A collar with a set screw is mounted on the rod and is used to set the desired height of the top of the lift and to prevent overcompaction of the lift.

Errors in Void Ratio Based on Specimen Measurements

The initial void ratio was determined based on the specimen weight and on measurements of the specimen diameter and height made at several discrete locations on the specimen. Because the steady state relationship is very sensitive to void ratio, the influence of measurement errors on the magnitude of the initial void ratio can provide some insight into the accuracy of void ratio determination for laboratory specimens, and consequently the accuracy of steady state relationship determination using triaxial tests. To better quantify these influences, the relationships between the measured parameters (specimen weight, diameter, and height) were examined. While the specimen diameter is not exactly constant with height, and the height is not exactly constant around the perimeter of the specimen, it is typically assumed that the specimen is a uniform right circular cylinder, and any variation in measured dimensions are averaged when calculating the initial void ratio of the specimen. Table 8.3 shows the relationships between variations in the measured dimensions and the resulting variations in the specimen area, volume, dry density, and void ratio assuming that the specimen is a uniform right circular cylinder.

Table 8.3 - Specimen Variations Due to Measured Dimension Variations

	$\frac{\partial}{\partial d}$	$\frac{\partial}{\partial h}$	$\frac{\partial}{\partial W}$
A	$\frac{1}{2}\pi d$	0	0
V	$\frac{1}{2}\pi dh$	$\frac{1}{4}\pi d^2$	0
γ_d	$-\frac{2\cdot\gamma_d}{d}$	$-\frac{\gamma_d}{h}$	$\frac{1}{V}$
e	$\frac{2\cdot G_S\cdot\gamma_w}{d\cdot\gamma_d}$	$\frac{G_S\cdot\gamma_w}{h\cdot\gamma_d}$	$-\frac{G_S\cdot\gamma_w}{W\cdot\gamma_d}$

where:
d = specimen diameter
h = specimen height
W = specimen weight
A = specimen area
V = specimen volume
γ_d = dry unit weight
e = void ratio
G_s = specific gravity of solids
γ_w = unit weight of water

Equation 8.1, Equation 8.2, and Equation 8.3 relate changes in diameter, height, and weight, respectively, to changes in initial void ratio.

$$\frac{\partial}{\partial d}e = \frac{2 \cdot G_S \cdot \gamma_w}{d \cdot \gamma_d} \qquad \text{Equation 8.1}$$

$$\frac{\partial}{\partial h}e = \frac{G_S \cdot \gamma_w}{h \cdot \gamma_d} \qquad \text{Equation 8.2}$$

$$\frac{\partial}{\partial W}e = -\frac{G_S \cdot \gamma_w}{W \cdot \gamma_d} \qquad \text{Equation 8.3}$$

where:
- e = void ratio
- d = specimen diameter
- h = specimen height
- W = specimen weight
- G_s = specific gravity of solids
- γ_w = unit weight of water
- γ_d = dry unit weight

Since the algebraic sign of measurement errors can be positive or negative, the contributions of Equation 8.1, Equation 8.2, and Equation 8.3 for small differential changes in diameter, height, and weight should be summed. Combining these three equations and changing the sign for the contribution due to errors in weight measurement results in:

$$\begin{aligned}\Delta e &= \frac{\partial e}{\partial d}\Delta d + \frac{\partial e}{\partial h}\Delta h + \frac{\partial e}{\partial W}\Delta W \\ &= \frac{G_S \gamma_w}{\gamma_d} \cdot \left(\frac{2}{d} \cdot \Delta d + \frac{1}{h} \cdot \Delta h - \frac{1}{W} \cdot \Delta W \right)\end{aligned} \qquad \text{Equation 8.4}$$

For a 2.8 inch diameter loose sand specimen (e = 0.797), the following dimensions and weight are typical:

d = 2.800 inches

h = 6.00 inches

W = 1.940 pounds

Substituting these typical values into Equation 8.4, and converting the weight in pounds to mass in grams results in Equation 8.5 as follows:

$$\Delta e = 1.283851 \cdot \frac{\Delta d}{in} + 0.2995652 \cdot \frac{\Delta h}{in} - 0.002042490 \cdot \frac{\Delta W}{g} \qquad \text{Equation 8.5}$$

Equation 8.5 shows that if the error associated with the measurement of each specimen dimension and the specimen mass are of the same order, the error in measurement of the diameter has the most significant influence on the accuracy of the calculated void ratio, and the error in determination of the specimen mass has the least significance. For the typical specimen dimensions noted, the variation in diameter, assuming no variation in height or mass, that results in a void ratio variation of 0.01 is 0.008 inches. Similarly, the variation in height, assuming no variation in diameter or mass, that results in a void ratio variation of 0.01 is 0.033 inches. Likewise, the variation in mass, assuming no variation in diameter or height, that results in a void ratio variation of 0.01 is 4.9 grams.

The specimen diameter was measured using a circumferential π-tape with a precision of 0.001 inches. The specimen height was measured using a steel machinist's rule with a precision of 0.01 inches. The mass of the specimen was measured on an electronic balance with a precision of 0.01 grams. Substituting the typical specimen dimensions into Equation 8.4 and using the precision of the instruments as the differential changes, the resulting variation in void ratio is $\pm$ 0.005. This variation is based on the assumption that the specimen is a perfectly uniform right circular cylinder, which is not necessarily the case. Further uncertainty in the determination of the initial void ratio can

arise from the fact that the specimens are not always perfectly uniform right circular cylinders, even if carefully prepared. Taking into account that the specimen may not be a perfect cylinder, and noting that the potential for error in measurement of the specimen mass can increase when each lift is measured independently, more reasonable estimates of the accuracy of the measured dimensions are:

$\Delta d = \pm 0.01$ inches

$\Delta h = \pm 0.05$ inches

$\Delta W = \pm 0.5$ grams

Substituting these variations in Equation 8.4, the resulting uncertainty in the calculated initial void ratio is $\pm$ 0.03. This uncertainty is significant enough to raise doubts about the accuracy of determining the steady state relationship based on laboratory tests when the void ratio is determined based on external measurements of the specimen dimensions with accuracies on the order of those previously noted.

Test Procedures

Once compaction of the last lift was complete, the top end platen was placed on the specimen, and the specimen dimensions were measured while maintaining an effective stress of 10 psi on the specimen by drawing a vacuum on the internal pores of the specimen. Figure 8.8 shows a typical specimen at this stage of the test. Specimen dimensions were measured and recorded at this point and the cell was assembled and filled. The cell pressure was increased from 0 psi to 10 psi while the vacuum was simultaneously decreased from 10 psi to 0 psi, so that a constant effective stress was maintained in the specimen. Minimizing the change in effective stress between the time the specimen dimensions are measured and the time when saturation is complete

will minimize the occurrence of volume change during this period, which cannot be measured.

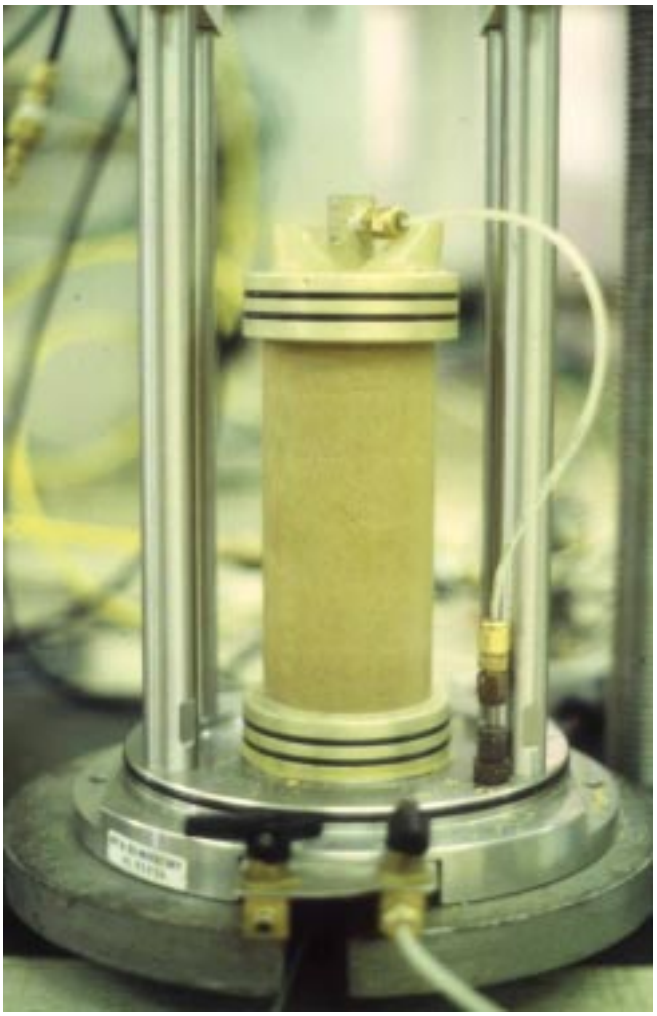

Figure 8.8 – Specimen with Internal Vacuum Applied

Saturation of the specimen was accomplished by first purging the specimen with carbon dioxide to displace as much air as possible out of the specimen voids. This method has been shown to improve the saturation of sand specimens (Lade and Duncan 1973). De-aired water was passed through the specimen under a small hydraulic head created by applying a slight vacuum to the top of the specimen and allowing the de-aired water to enter through the

bottom platen. In most cases, the amount of de-aired water allowed to pass through the specimen was approximately twice the total volume of the specimen. Both the top and bottom drainage lines were then connected to the pore pressure board and the specimen was saturated completely by applying equal increments of back pressure and cell pressure to the specimen. In most cases, specimens were nearly saturated prior to the application of any back pressure, and complete saturation could be accomplished with only modest application of back pressure (10 psi to 30 psi). Saturation was considered to be acceptable when the value of the pore pressure parameter B was 0.98 or greater, although in most instances, values greater than 0.99 were achieved. All specimens were consolidated for at least 30 minutes, but primary consolidation was typically complete after shorter periods of time due to the high values of permeability associated with the clean sands that were tested. The specimens were sheared by applying an axial load at a constant rate of displacement. Figure 8.9 shows a typical specimen at small strain levels, just after the onset of the shear phase of the test. Figure 8.10 shows a specimen with lubricated ends at the onset of some nonuniform deformation. Even when lubricated ends were used, some nonuniform deformation was often observable at intermediate strain levels. Typical specimen conditions at large strain levels after failure on a shear surface and failure by bulging are shown in Figure 8.11 and Figure 8.12, respectively. In general, the use of lubricated ends resulted in the eventual development of a shear surface, while the use of conventional ends resulted in either type of condition after failure. The shear phase of the test was carried out until steady state conditions were achieved or until some deviation of conditions occurred that obviously precluded the usefulness of the test data. Examples of such deviations are significant bending of the loading piston, severe tilting of the top end platen, and contact between the specimen and the triaxial cell in cases where extreme deformation was observed.

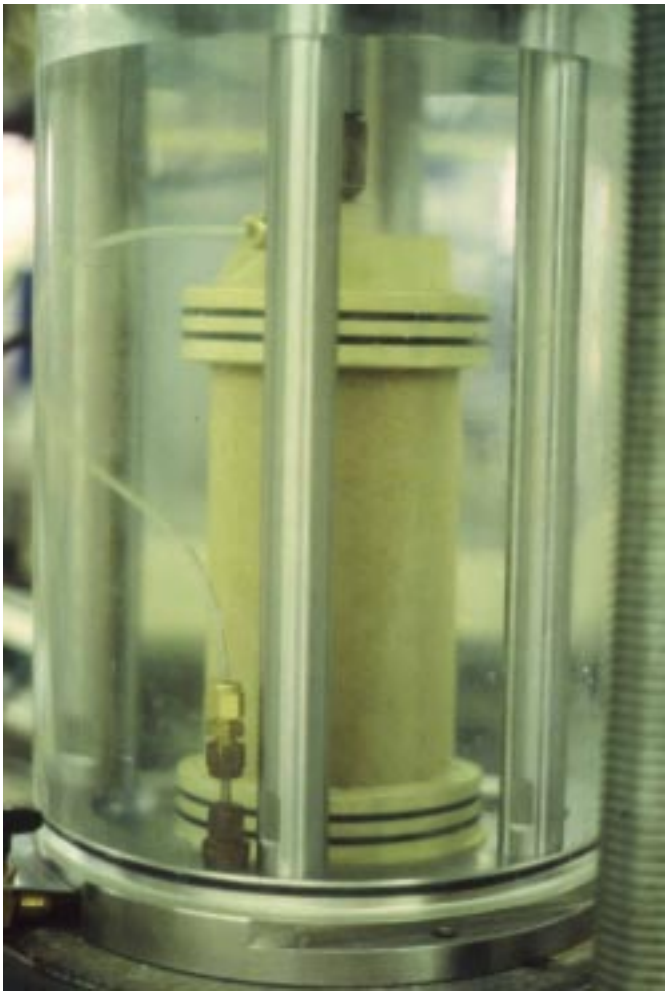

Figure 8.9 – Specimen Condition at Small Strain Levels

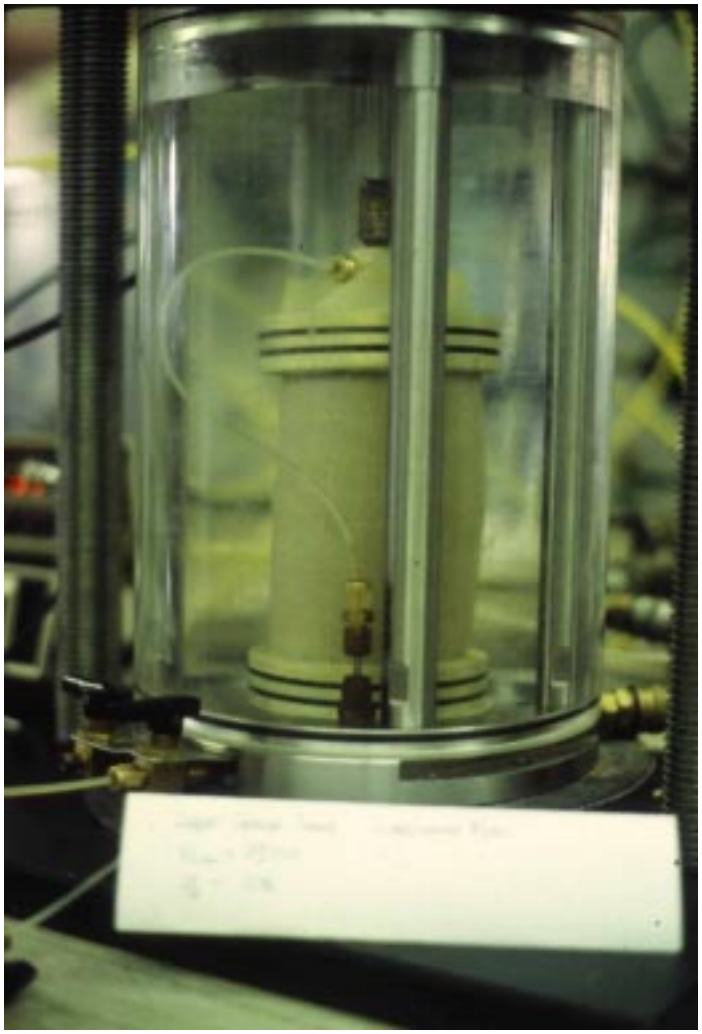

Figure 8.10 – Specimen Condition at Intermediate Strain Levels

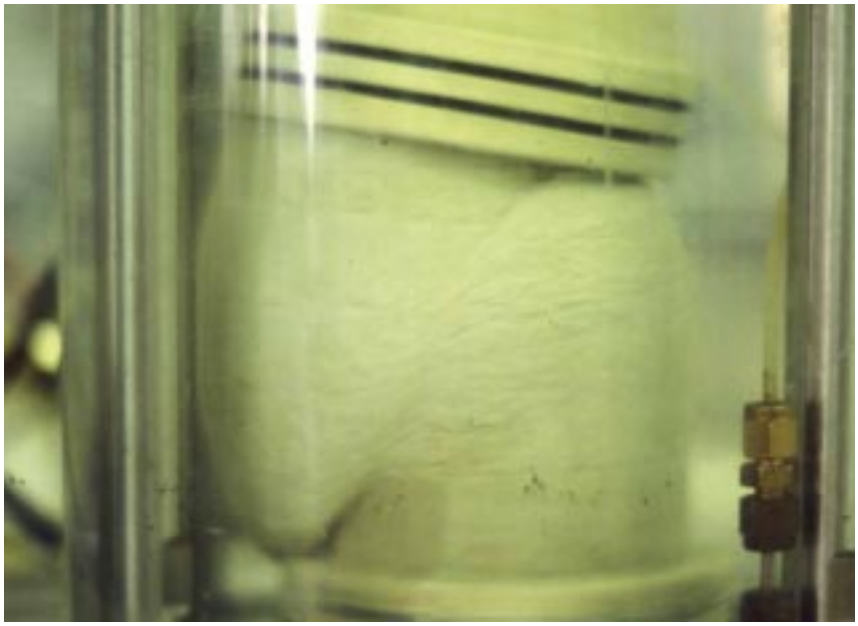

Figure 8.11 – Specimen Condition After Shear Plane Failure

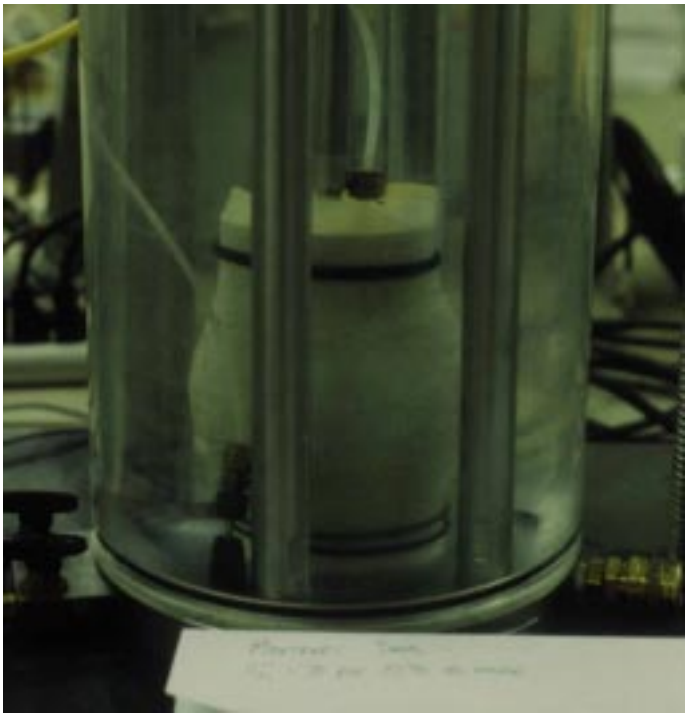

Figure 8.12 – Specimen Condition After Bulging Failure

Test Data Reduction

The raw data collected for each test consisted of the axial displacement, axial deviator force, and effective confining stress, or difference in cell pressure and internal pore water pressure. The axial displacement is converted to axial strain by dividing by the assumed specimen height after consolidation. The axial deviator stress is calculated based on the measured force and the assumed cross-sectional area of the specimen. To demonstrate the influence of the various corrections on calculated stresses and derived parameters, the results from one test can be examined. Figure 8.13 shows the measured axial force and calculated deviator stresses based on various deformation modes and corresponding area corrections. Application of the parabolic or sinusoidal area correction results in very similar deviator stresses, while the RCC correction results in a deviator stress greater than that based on nonuniform bulging. Figure 8.13 also demonstrates that the significance of the area correction with respect to the calculated deviator stress increases as axial strain increases. The influence of the area corrections on the effective stress path and principal stress ratio is demonstrated in Figure 8.14. The effect on the stress path is insignificant prior to failure, defined by the maximum principal stress ratio. After failure, however, the assumed area correction has a significant effect on the calculated stress path. As was the case with the deviator stress, the effect becomes more significant as strain increases.

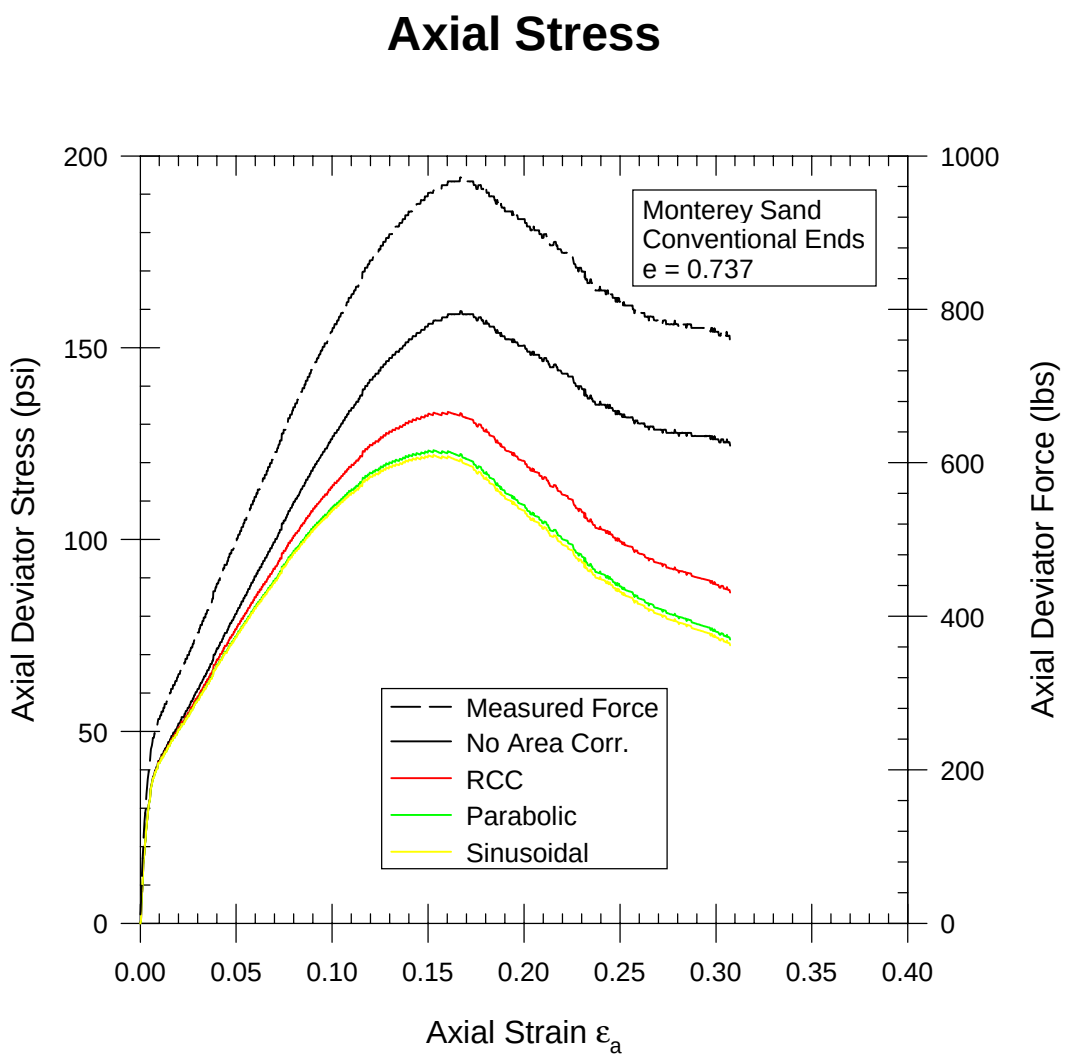

Figure 8.13 - Influence of Area Correction on Calculated Deviator Stress

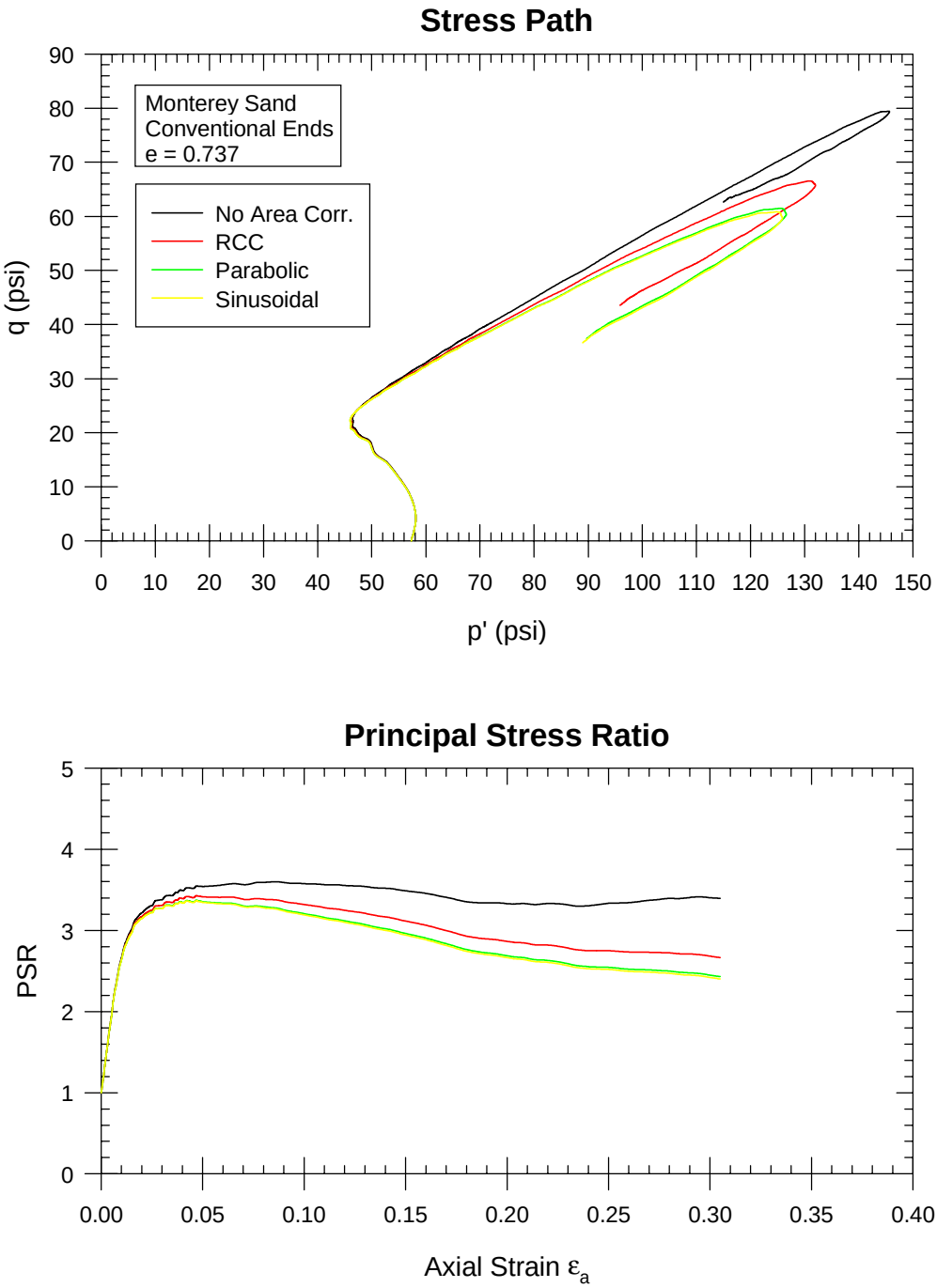

Figure 8.14 - Influence of Area Correction on Stress Path and Principal Stress Ratio

Figure 8.15 and Figure 8.16 demonstrate the influence of applying the membrane stress corrections to the test data. The reduction in the deviator

stress for both modes of deformation is detectable but minimal. The increase in the confining stress for the parabolic bulging case is insignificant. Since the correction to the confining stress is equal to zero for RCC deformation and zero volume change, the variation of confining stress for RCC deformation with and without the membrane correction is identical to that for parabolic bulging without the correction. The effects of applying the membrane stress corrections on the calculated stress path and principal stress ratio appear to be negligible for both modes of deformation, as shown in Figure 8.16.

The results of the CU tests performed were reduced based on both RCC deformation and parabolic bulging with membrane stress corrections applied. Since results based on sinusoidal bulging are so similar to those based on parabolic bulging, the sinusoidal bulging corrections were not applied. Plots of principal stresses, deviator stress, bulk stress, principal stress ratio, and the stress path for each test are provided in Appendix G.

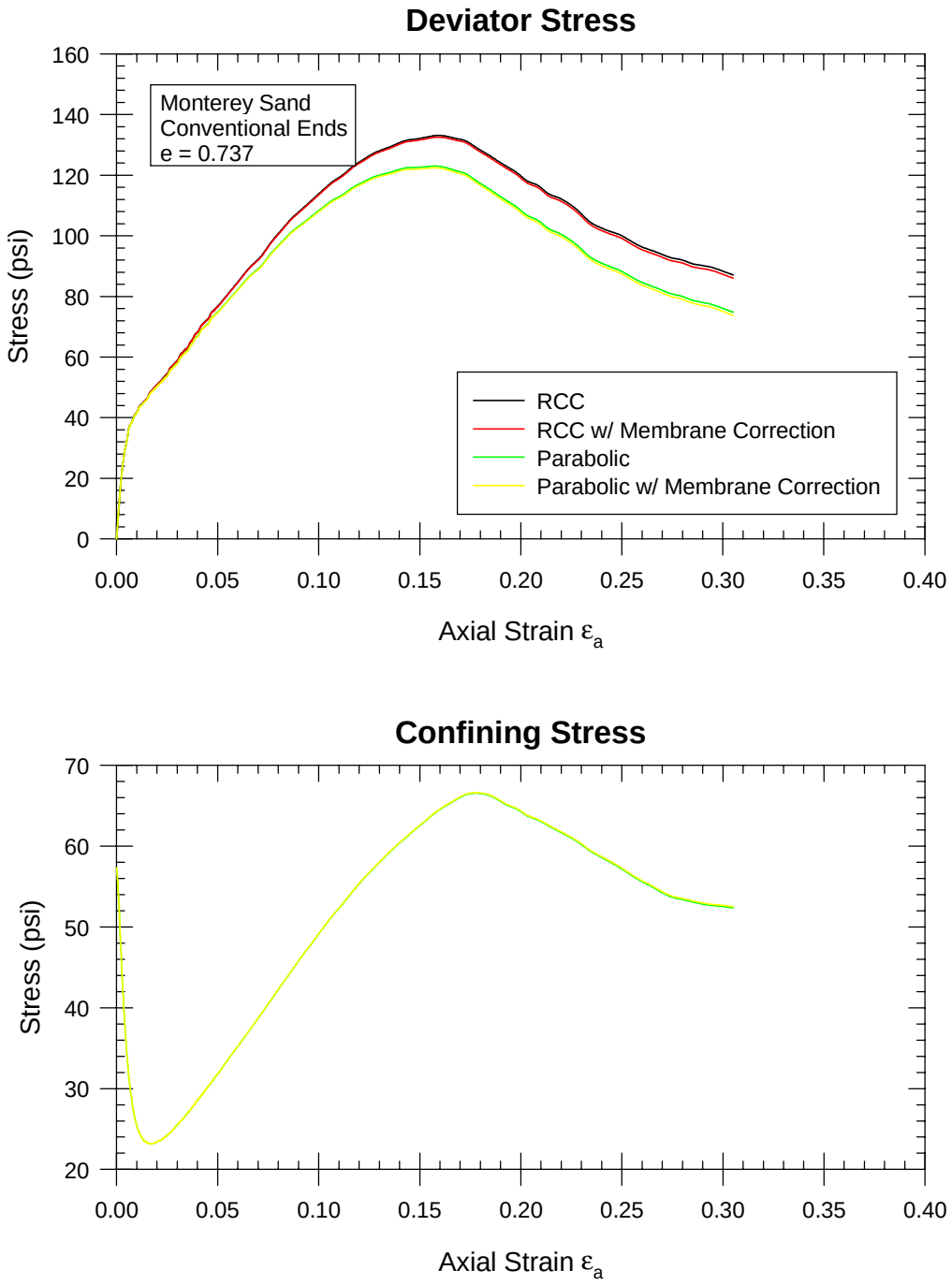

Figure 8.15 - Influence of Membrane Correction on Specimen Stresses

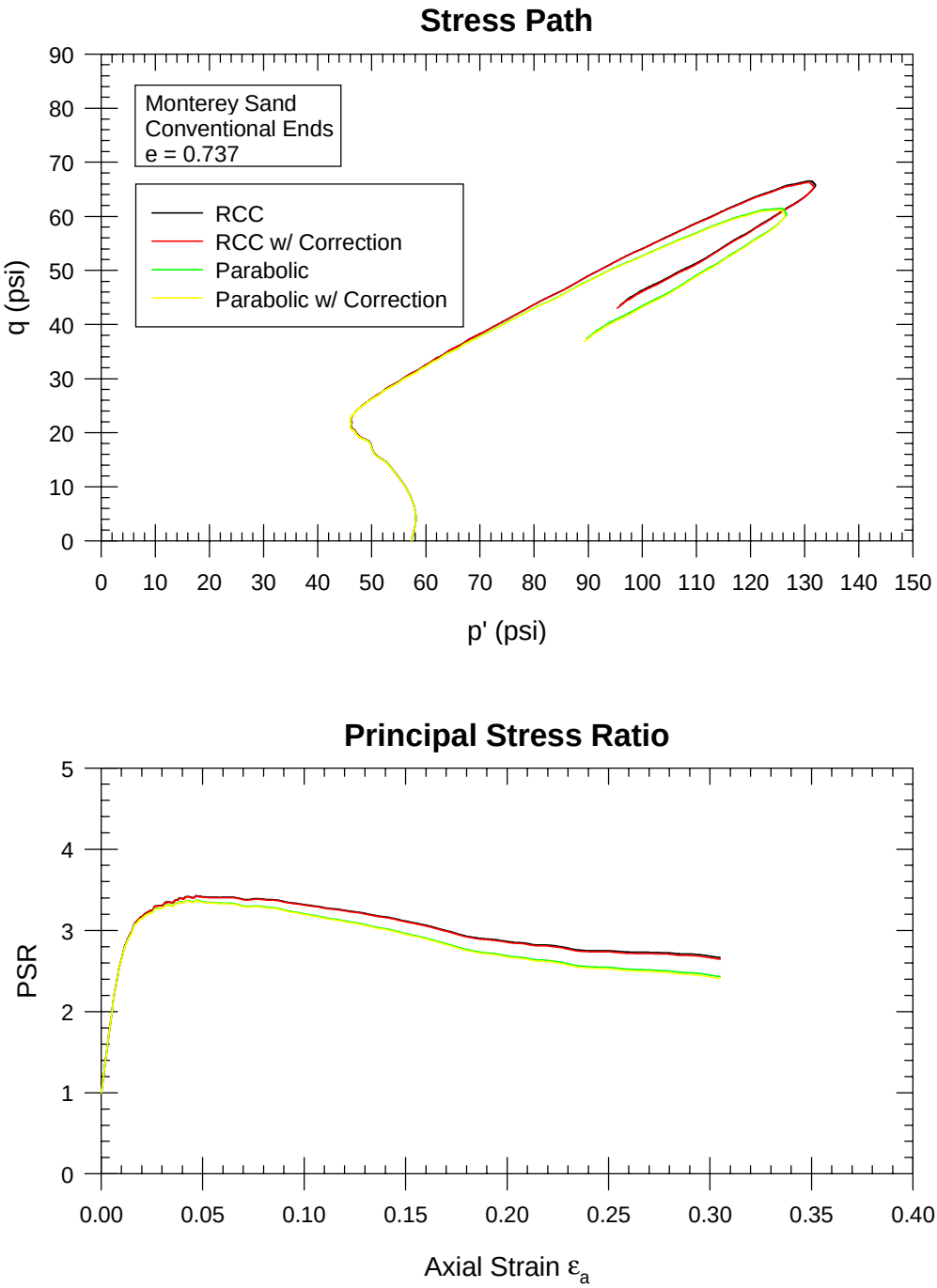

Figure 8.16 - Influence of Membrane Correction on Stress Path and Principal Stress Ratio

Comparison of Lubricated and Conventional Ends

In some cases, tests were performed on samples with identical void ratios using both conventional and lubricated end platens to allow direct comparison of results. These results provide experimental comparisons to compliment the analytical comparisons described in Chapter 7. The stress-strain behavior for two specimens of Light Castle Sand corresponding to a relative density of approximately one percent is compared in Figure 8.17. The parabolic area correction was applied to the data for both specimens. The effective confining stress for the specimen using conventional ends decreases to a minimum value slightly greater than the minimum value for the specimen with lubricated ends, then begins to increase at greater strain levels. The deviator stress for the specimen using conventional ends is greater than that for the specimen using lubricated ends throughout the range of strain in the test. The initial peak is approximately 10% greater for the specimen with conventional ends. At larger strain levels, the deviator stress increases for the specimen with conventional ends, but not for the specimen with lubricated ends. The difference between the measured stresses increases as the axial strain increases. Although the stress-strain relationship is more complex than those modeled by the finite element method, the effects of end restraint on the stress-strain behavior demonstrated by the experimental results are in general agreement with those based on the analytical results.

Figure 8.18 shows the stress paths and principal stress ratios for the same two tests. The general shape of the stress paths are very similar, but the specimen with conventional end platens exhibited a significant increase in deviator stress after failure, shown in Figure 8.18 by the stress path tracing the failure envelope. The behavior was not observed for the specimen using lubricated end platens. The principal stress ratio was greater for the specimen using conventional ends at all strain levels.

The results of tests on two specimens of Ottawa Sand corresponding to a relative density of approximately 13% are compared in Figure 8.19 and Figure 8.20. Although the two specimens were consolidated to different effective stress levels, the results indicate the same effects based on the use of lubricated end platens. Since the specimen using conventional ends was consolidated to a higher effective stress, the difference in peak deviator stress is much greater than would be expected based solely on the end conditions. The difference in effective confining stress does not become significant until an axial strain level of approximately 10% for this set of tests. Again, the stress path for the specimen using conventional ends exhibits an increase in stress level after failure while the specimen with lubricated ends does not. The difference in principal stress ratio, which is much greater for this set of tests, is due partially to the end effects, but may be of questionable accuracy due to the sensitivity of the principal stress ratio to the extremely low effective stress levels observed in both tests. Comparison of similar tests at nearly identical void ratios demonstrates similar results and observations about the effect of using lubricated end platens. In general, the experimental results support the analytical results described in Chapter 7. The friction on the specimen ends resulting from the use of conventional end platens results in an apparent increase in the measured stresses. The magnitude of the difference in results based on conventional ends and lubricated ends increases as strain level increases. The effect of the end friction may be negligible at strain levels corresponding to peak deviator stresses or failure based on the Mohr-Coulomb criterion, but is significant at greater strain levels.

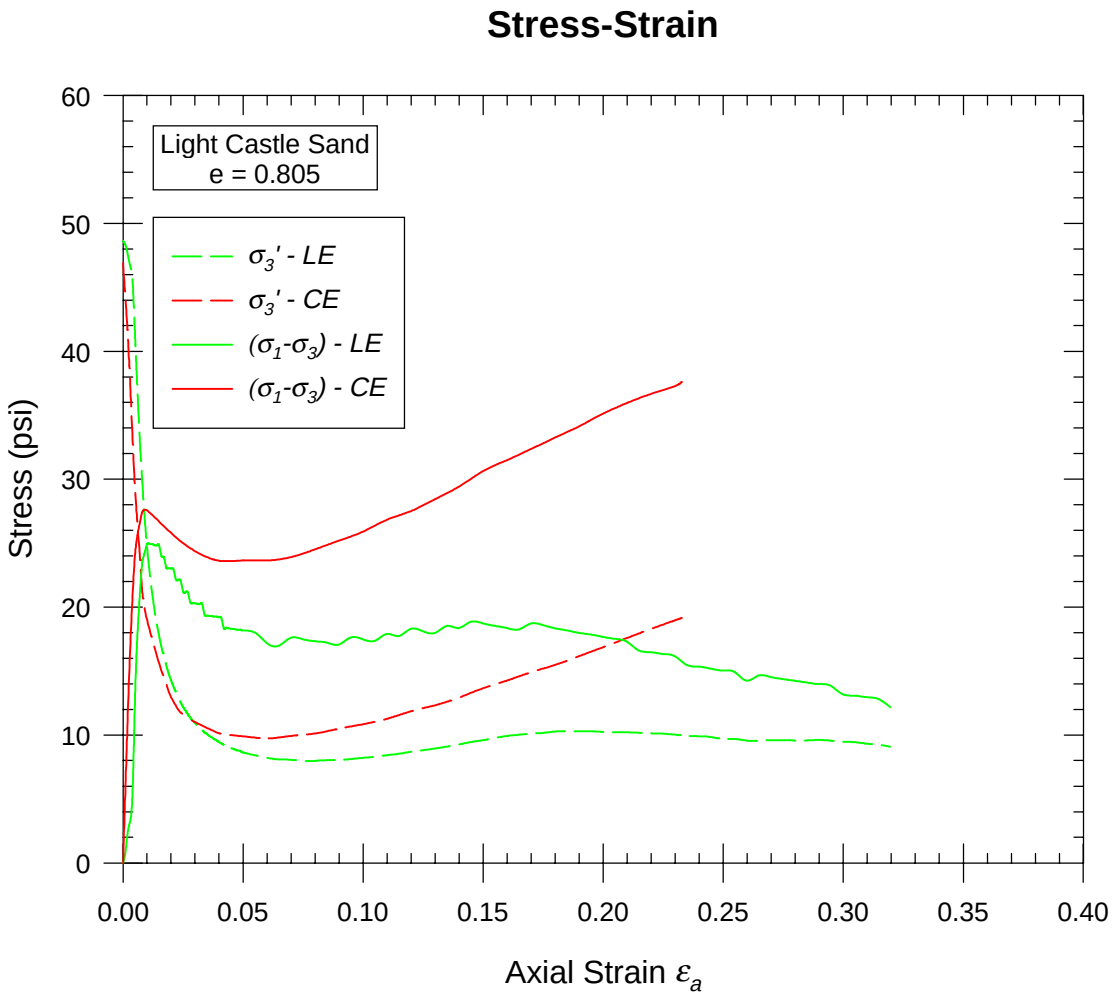

Figure 8.17 - Influence of End Condition on Stress-Strain Behavior for Light Castle Sand

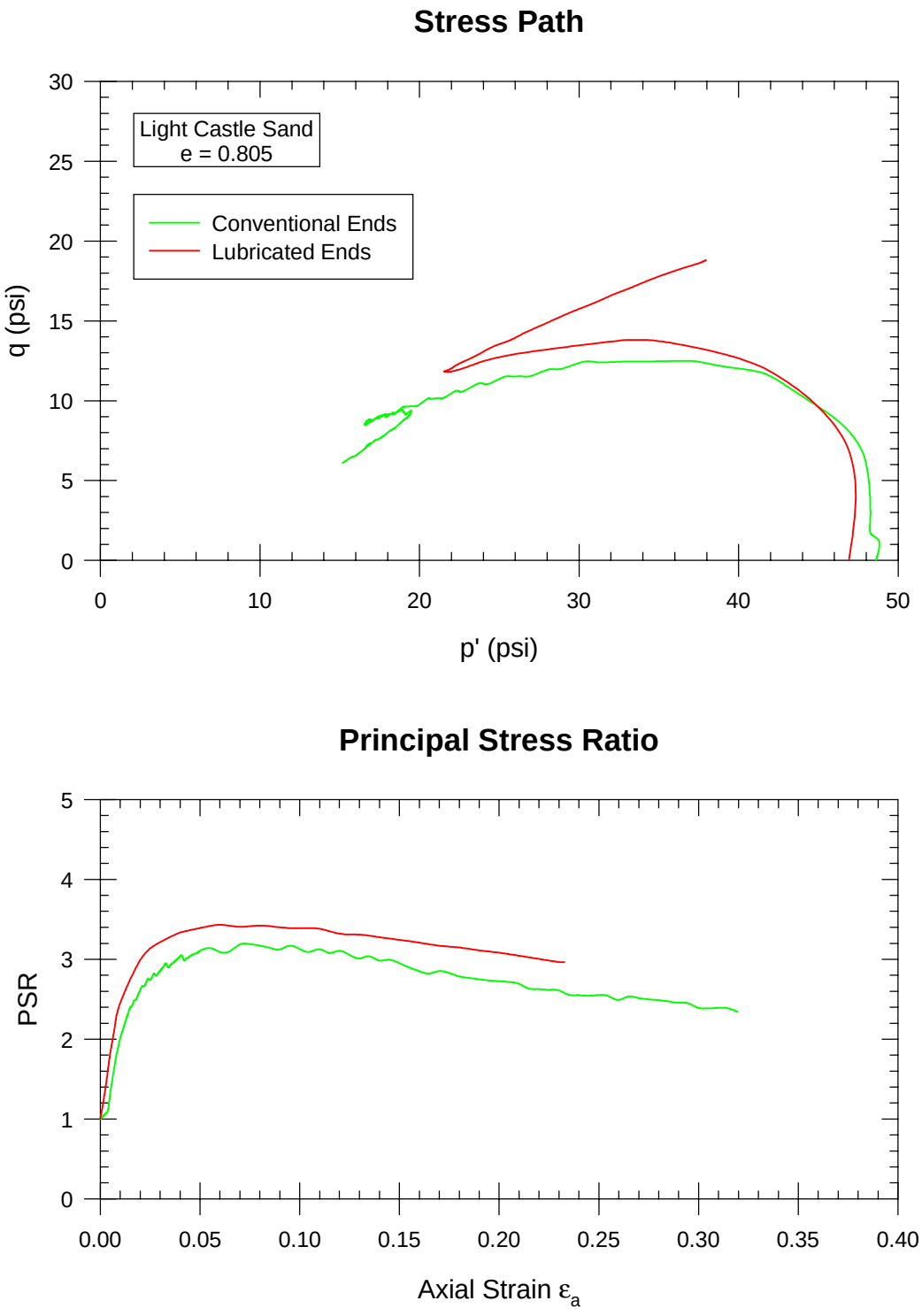

Figure 8.18 - Influence of End Condition on Stress Path and Principal Stress Ratio for Light Castle Sand

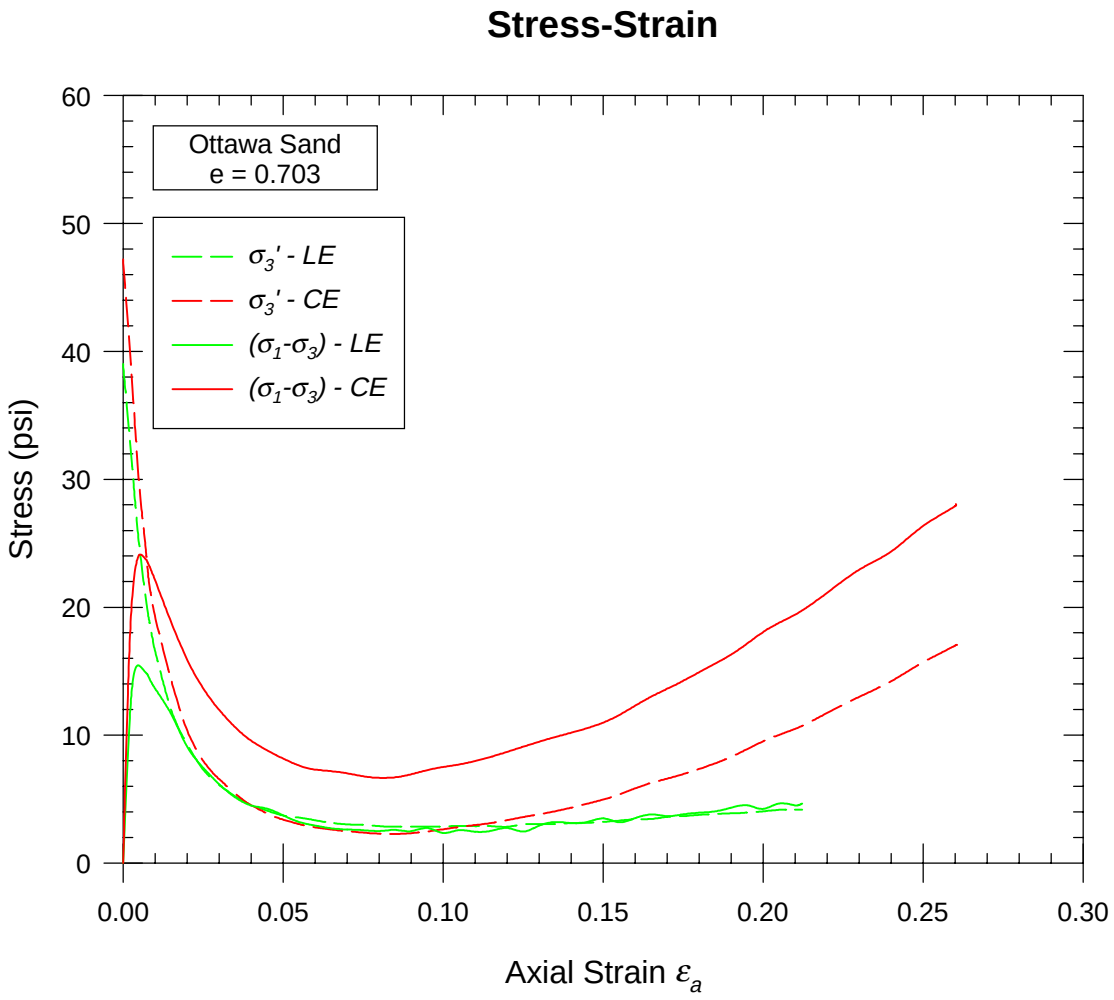

Figure 8.19 - Influence of End Condition on Stress-Strain Behavior for Ottawa Sand

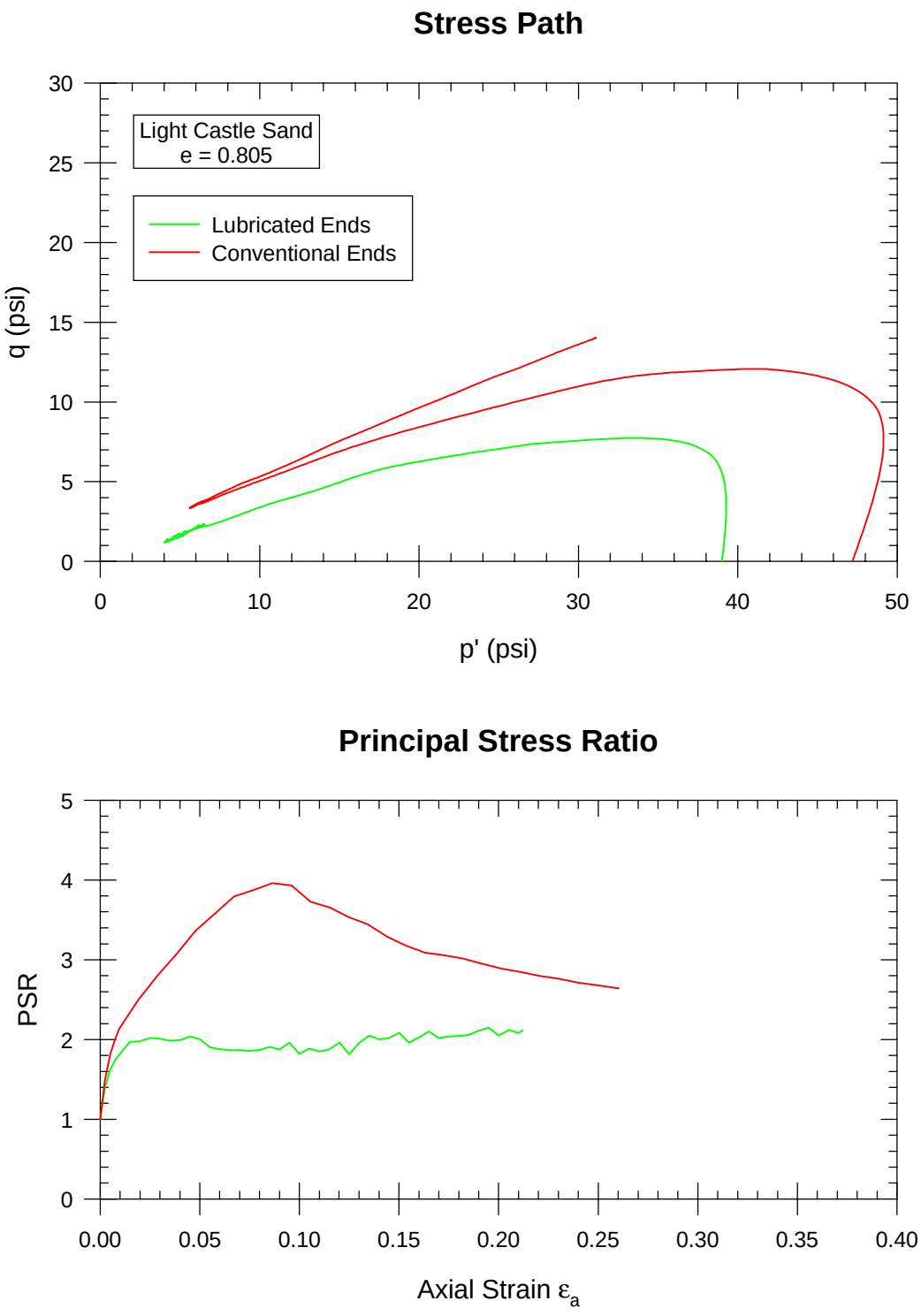

Figure 8.20 - Influence of End Condition on Stress Path and Principal Stress Ratio for Ottawa Sand

Relationships Among Steady State Parameters

As noted in Chapter 2, the steady state relationship has been characterized using various parameters to represent either the effective stress at steady state or the steady state undrained shear strength. The minor principal effective stress has been used since the definition of steady state includes the requirement that the effective stress be constant. The first principal stress invariant (J_1'), which is the sum of the effective principal stresses has also been used (Been and Jefferies 1985). The mean effective stress in two dimensions (p') was used by Alarcon-Guzman et al. (1988). These parameters are distinct but interrelated measures of the effective normal stress level of the soil. The shear stress level can also be used to characterize the steady state relationship. The maximum shear stress at steady state (q), or the steady state undrained shear strength (S_{us}) defined as the shear stress on the failure surface have both been used (Castro et al. 1982, Poulos et al. 1985). If the effective principal stresses at steady state conditions are known any of the representations can be used. The relationships between the various parameters were outlined in Chapter 2.

If the slope of the steady state line based on any of the parameters is constant, then the slope based on each of the parameters will be constant. Furthermore, if the cohesion intercept for the steady state strength envelope is equal to zero and the steady state friction angle is constant, the slopes of the steady state lines based on any of the stress parameters mentioned will be identical. However, the position of the lines will differ depending on which measure is employed. For a particular stress level, the void ratio corresponding to the steady state line for each measure of stress will be offset from the steady state void ratio based on the minor principal effective stress by an amount Δe. If the steady state cohesion intercept is equal to zero, the offsets are described by the following equations:

$$\Delta e_{p'} = \lambda_{ss} \cdot (1 - \sin\phi'_{ss}) \qquad \text{Equation 8.6}$$

$$\Delta e_{J_1'} = \lambda_{ss} \cdot \left(\frac{1 - \sin\phi'_{ss}}{3 - \sin\phi'_{ss}} \right) \qquad \text{Equation 8.7}$$

$$\Delta e_{q} = \lambda_{ss} \cdot \left(\frac{1 - \sin\phi'_{ss}}{\sin\phi'_{ss}} \right) \qquad \text{Equation 8.8}$$

$$\Delta e_{S_{us}} = \lambda_{ss} \cdot \left(\frac{1 - \sin\phi'_{ss}}{\sin\phi'_{ss} \cdot \cos\phi'_{ss}} \right) \qquad \text{Equation 8.9}$$

where: Δe = steady state void ratio offset based on σ'_3
λ_{ss} = slope of steady state line in log (stress) space
ϕ'_{ss} = steady state friction angle

An example of the relationship between the various means of characterizing the steady state line is shown in Figure 8.21. The lines based on p' and J'_1 will always lie above the line based on σ'_3 while the position of the lines based on q and S_{us} depend on the value of the steady state friction angle. If the value of ϕ'_{ss} is equal to 30°, then the steady state lines based on q and σ'_3 will be identical. Likewise, if the value of ϕ'_{ss} is equal to 32.94°, then the steady state lines based on S_{us} and σ'_3 will be identical. The steady state line based on either of the shear strength parameters will lie above the line based on σ'_3 if the value of ϕ'_{ss} is greater than the associated characteristic value noted above. If the value of ϕ'_{ss} is less than the associated value above, the steady state line based on either q or S_{us} will lie below the line based on σ'_3. Since the primary goal of conducting CU triaxial tests in the liquefaction susceptibility evaluation procedure outlined by Poulos et al. (1985) is to determine the slope of the steady state line, any of the measures of stress discussed should yield equally appropriate results.

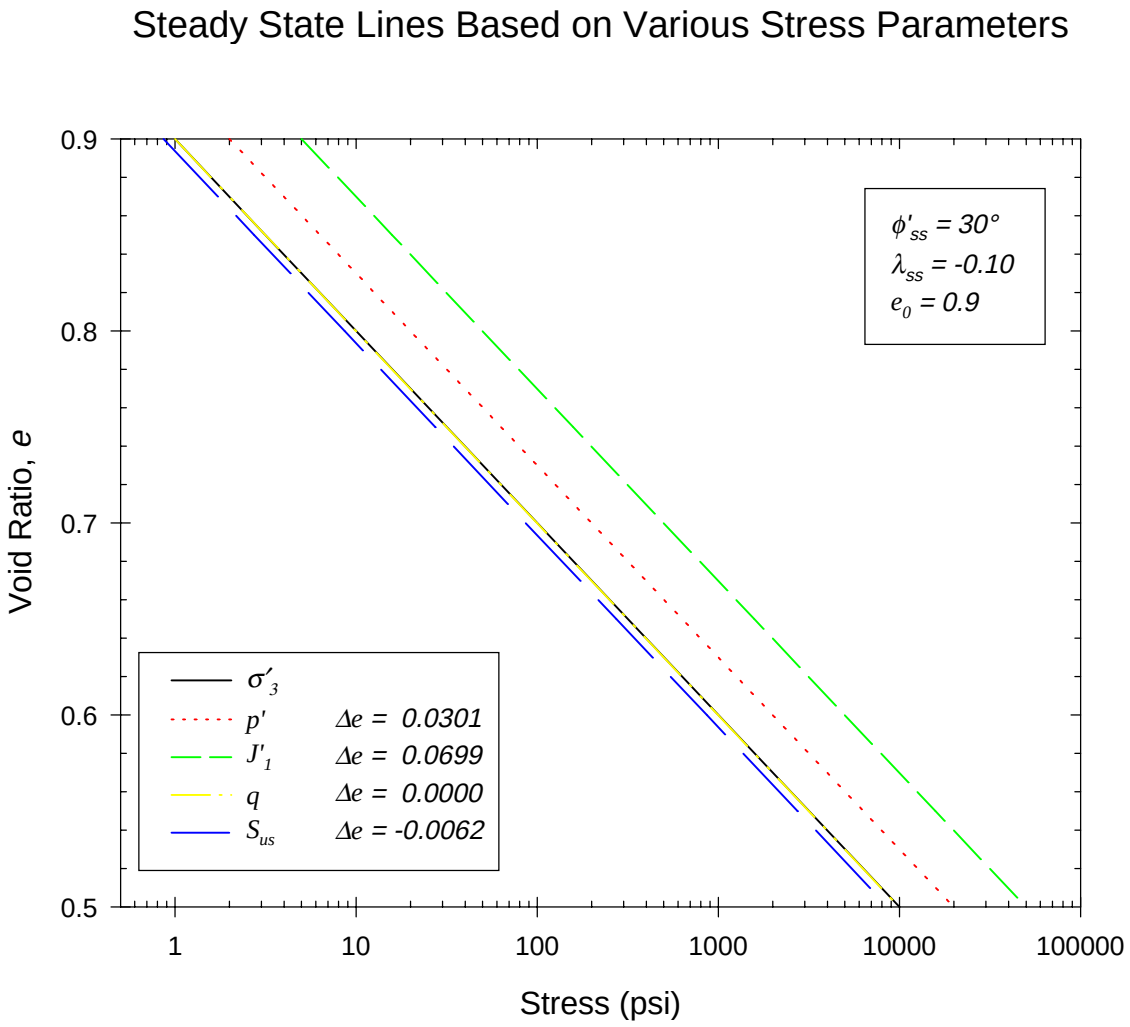

Figure 8.21 – Steady State Lines Based on Various Stress Parameters

Determination of Steady State in Test Data

As noted earlier, the axial load and internal pore pressure were measured, as is typical, during the shear phase of the CU triaxial tests performed for this study. The pore pressure was measured using a differential pressure transducer that compared the internal pore pressure to the applied cell pressure. The output from this transducer is equal to the cell pressure minus the internal pore pressure, which is equivalent to the minor principal effective stress if the cell

pressure is equal to the minor principal total stress. This may not be the case at all locations within the specimen, since membrane effects and the effects of end friction can alter the stress state at different points throughout the specimen. Since the differential pressure transducer measures the difference in the cell pressure and the internal pore pressure very accurately, the measured minor principal effective stress likewise should be very accurate, provided that the cell pressure is indeed representative of the minor principal total stress throughout the specimen and that the pore pressure distribution within the specimen is nearly uniform. The measurement of the minor principal effective stress is not directly dependent on the measurement of the axial load or the axial deformation. For this reason, the minor principal effective stress should provide an accurate means of interpreting the triaxial test data and identifying the occurrence of steady state deformation.

All other means of characterizing steady state require the determination of the axial stress in the specimen. The axial stress is calculated based on the measured axial load and the cross-sectional area of the specimen. As a result, the axial stress is influenced by which area correction and which membrane correction, if any, is used. In addition, the measurement of the axial load can be influenced by piston friction, tilting of the end platen, and eccentricity due to bending of the piston when tests are carried out to very large strain levels. For these reasons, it is believed that a greater possibility for error exists in calculation of the axial stress than in determination of the minor principal effective stress based on measured test data.

When attempting to identify the steady state conditions based on the triaxial test data, plots such as that shown in Figure 8.22 were examined. The plot in Figure 8.22 shows the variation of the minor principal effective stress, the deviator stress, the major principal effective stress, and the sum of the principal effective stresses (first principal effective stress invariant) with

increasing axial strain. In an ideal steady state of deformation, all stress components should essentially become constant, as shown in Figure 8.22, but test data indicate that this is not always the case. Figure 8.23 shows the results of a test in which the minor principal effective stress becomes constant at approximately 15 percent axial strain, but the stresses that depend on calculation of the axial stress are only constant briefly and continue to vary again at approximately 19 percent axial strain. This phenomenon is likely attributable to inaccurate assumptions regarding the calculation of the axial stress or the nonuniformity of stress conditions that may occur at large strain levels. For example, if the axial load and the cross-sectional area of the specimen remained constant at strain levels greater than 19 percent, but the area correction used to reduce the data assumed that the cross-sectional area was increasing, the calculated axial stress would appear to decrease even though the true axial stress was constant. Stress nonuniformity can result in the measured axial force varying even though the stresses throughout most of the specimen do not. As a result, the average stresses based on external measurement can change while the stress state throughout most of the specimen remains constant.

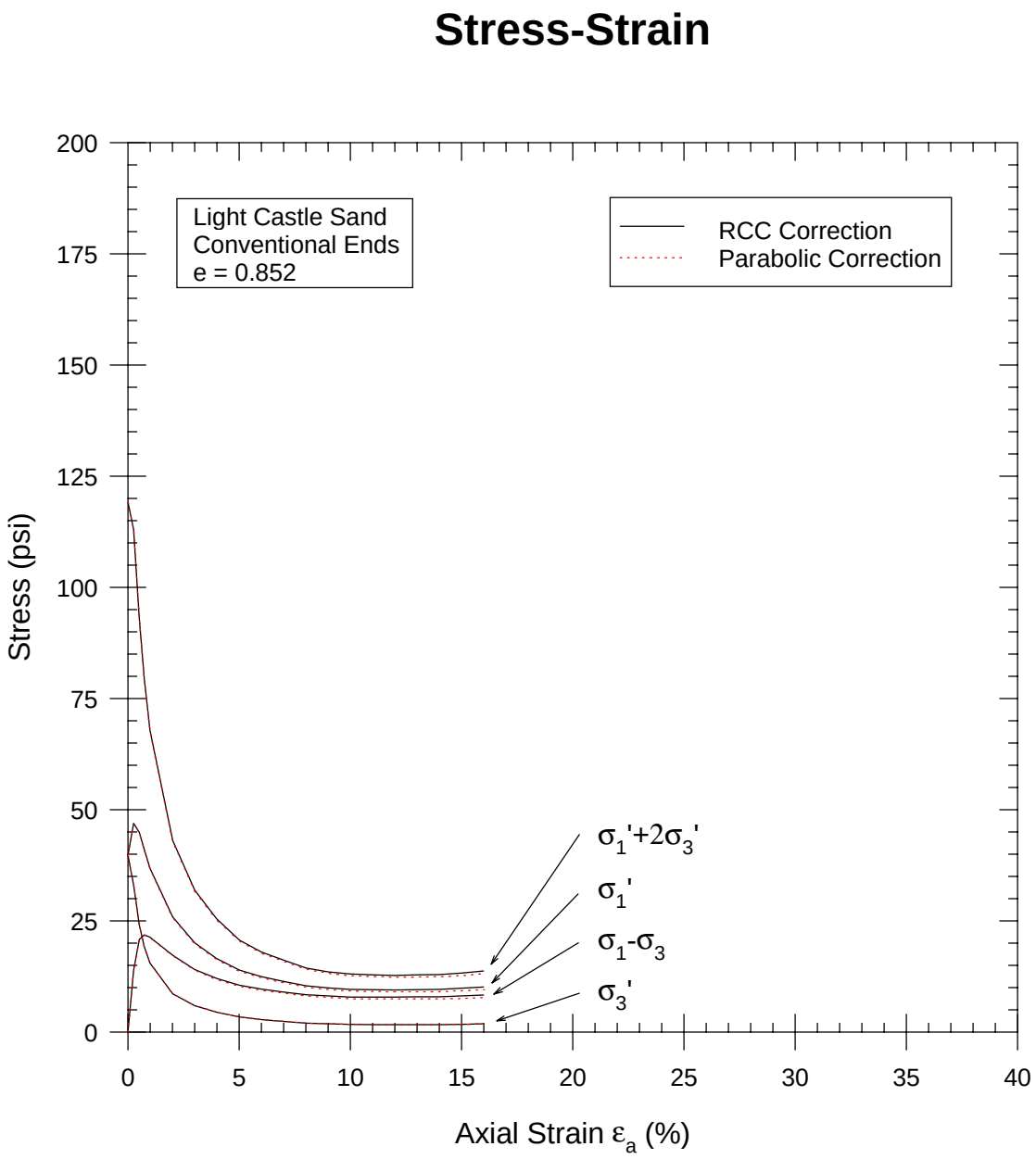

Figure 8.22 - Variation of Stresses with Axial Strain When All Stresses Become Essentially Constant

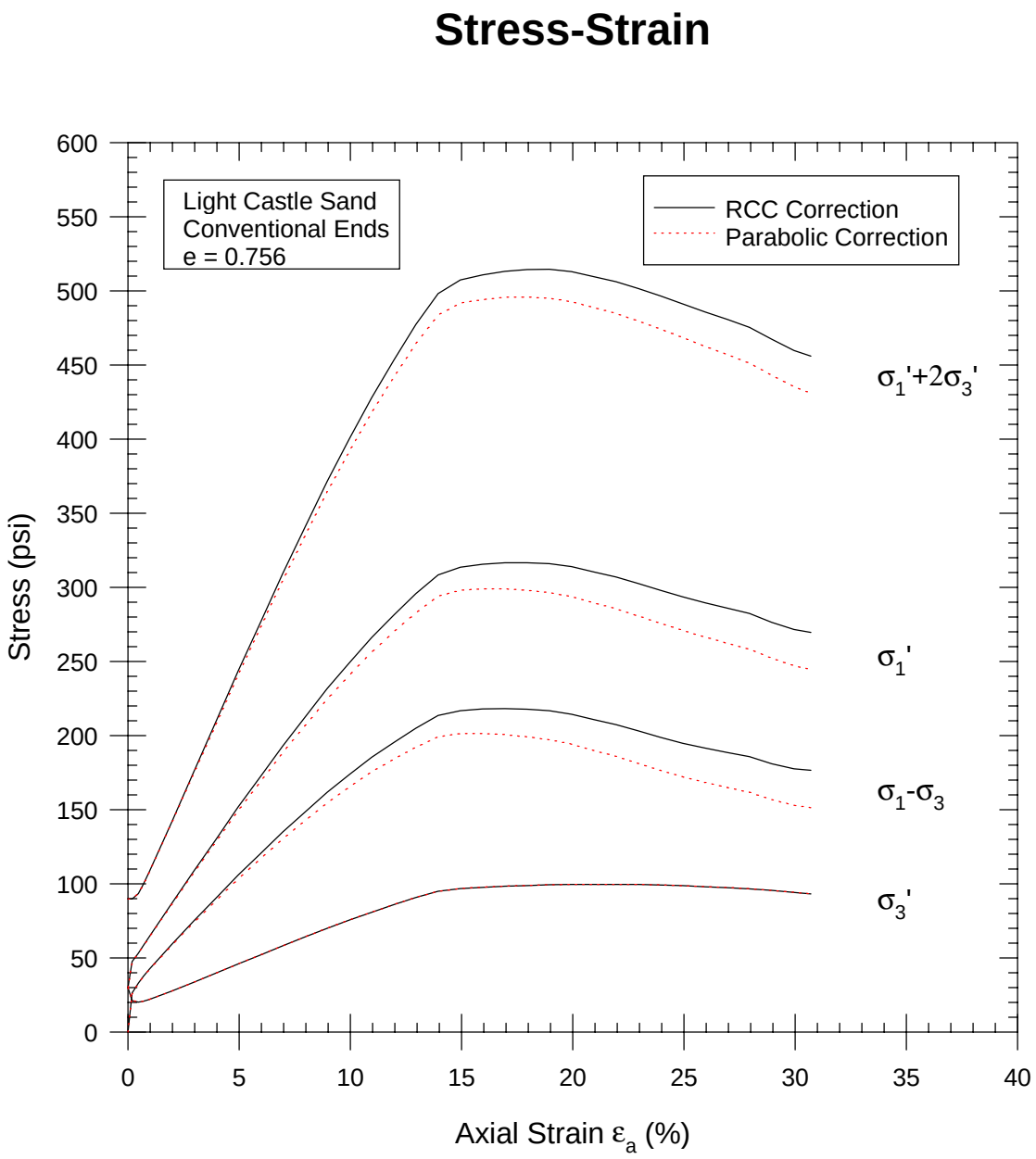

Figure 8.23 - Variation of Stresses With Axial Strain When All Stresses Do Not Become Constant

As a result of the possibility for error in calculation of the axial stress, greater emphasis was placed on the variation of minor principal effective stress with

strain when determining the occurrence of steady state deformation conditions based on measured test data. The steady state relationships are based on the minor principal effective stress, again since this value is affected only by the membrane correction for nonuniform bulging, which has been shown to be negligible for the specimen and membrane geometry associated with the tests performed in this study. The steady state relationship based on the first effective stress invariant or on the steady state undrained shear strength are influenced by the area correction used, and as such, are likely to be less accurate. Two conditions were identified based on the test data. The first was the occurrence of the minimum effective confining stress, which typically occurred at moderate strain levels and is referred to as the $\sigma_{3'min}$ condition. This condition has been used previously to characterize the steady state and has been described as the *quasi-steady state,* the *phase of transformation,* and *limited liquefaction* (Ishihara 1985, Alarcon-Guzman et al. 1988, Castro 1991, Ishihara 1993). The increase in stress level often observed after reaching the minimum value may be attributable to test conditions and not actual material response, so that the specimen would exhibit steady state behavior at this stress level if the constraints of the test could be removed. Furthermore, even if the observed behavior does represent the actual material response of the specimen, the inherent development of nonuniform conditions in the specimen at large strain levels, regardless of the end conditions, may mask the true steady state response and result in the apparent increase in stress level. The second condition is the apparent occurrence of constant stress levels occurring at much larger strain levels. Some specimens appeared to reach steady state conditions at very large strain levels and at stress levels different than those corresponding to the minimum effective stress condition. Other specimens did not appear to reach true steady state conditions, but did exhibit a small range of strain during which the stresses were essentially constant, often corresponding to the maximum measured deviator stress for the test. This

second condition is referred to as the steady state condition, although the actual steady state relationship for the material may be more accurately represented by the minimum effective stress condition for the reasons previously discussed.

Steady State Relationships

For each material, both conditions were identified for the tests using both conventional and lubricated end platens. Steady state relationships were determined separately for the results of tests using conventional ends and lubricated ends for both the minimum effective stress condition and the steady state condition. Figure 8.24 shows the steady state relationships for Light Castle sand. The intercept and slope of each line is also shown. Based on the procedure for liquefaction susceptibility evaluation developed by Poulos et al. (1985) and described in Chapter 2, the slope of the line (λ_{ss}) is the key parameter to be determined by the CU triaxial tests. For both the conventional end tests and the lubricated end tests the slope of the steady state line based on the minimum effective stress condition is greater than that based on the steady state condition by approximately 30 percent. For the relationships based on each condition, the slope of the steady state line is greater for the lubricated end test series than for the conventional end test series.

The steady state relationships for Monterey sand are shown in Figure 8.25. For this material, the relationships based on the steady state condition are nearly identical for both the lubricated end tests and the conventional end tests. The slope of the steady state line based on the minimum effective stress condition using lubricated end platens was less than that based on the steady state condition. In contrast, the slope of the steady state line based on the minimum effective stress condition using conventional end platens was greater

than that based on the steady state condition. Of all the relationships determined, this line exhibited the greatest slope.

Figure 8.26 shows the steady state relationships for Ottawa sand based on the tests performed. The steady state lines for Ottawa sand have nearly identical slopes regardless of which condition is used to determine the occurrence of steady state. The slope, however, is significantly influenced by the end conditions during the tests. The slope based on tests using lubricated end platens is approximately 2.5 to 3 times greater than that based on tests using conventional end platens.

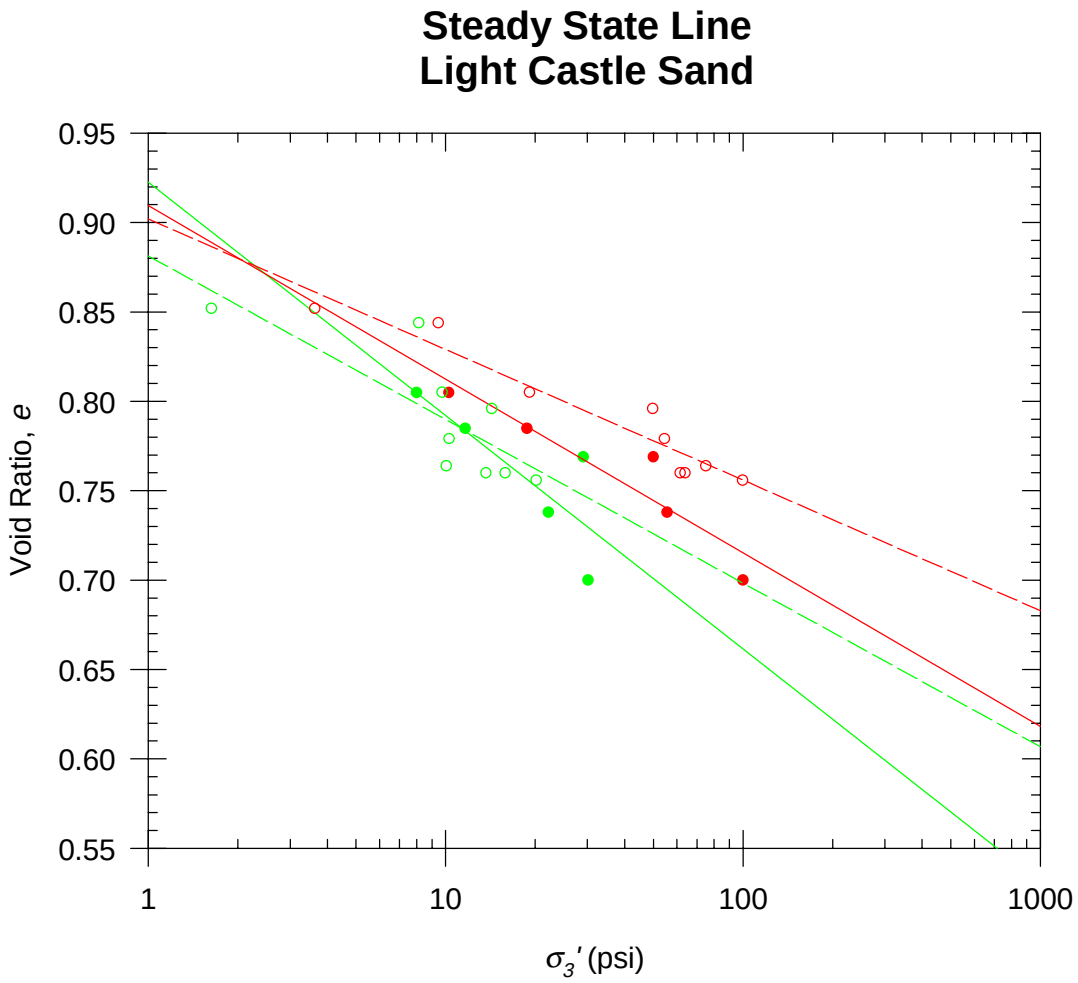

	Intercept	Slope
$\sigma_{3\,min}'$ - LE	0.922	-0.1305
SS - LE	0.910	-0.0971
$\sigma_{3\,min}'$ - CE	0.881	-0.0915
SS - CE	0.902	-0.0731

$\sigma_{3\,min}'$ - Lub. Ends
$\sigma_{3\,min}'$ - Lub. Ends
Steady State - Lub. Ends
Steady State - Lub. Ends
$\sigma_{3\,min}'$ - Conv. Ends
$\sigma_{3\,min}'$ - Conv. Ends
Steady State - Conv. Ends
Steady State - Conv. Ends

Figure 8.24 - Steady State Relationship for Light Castle Sand

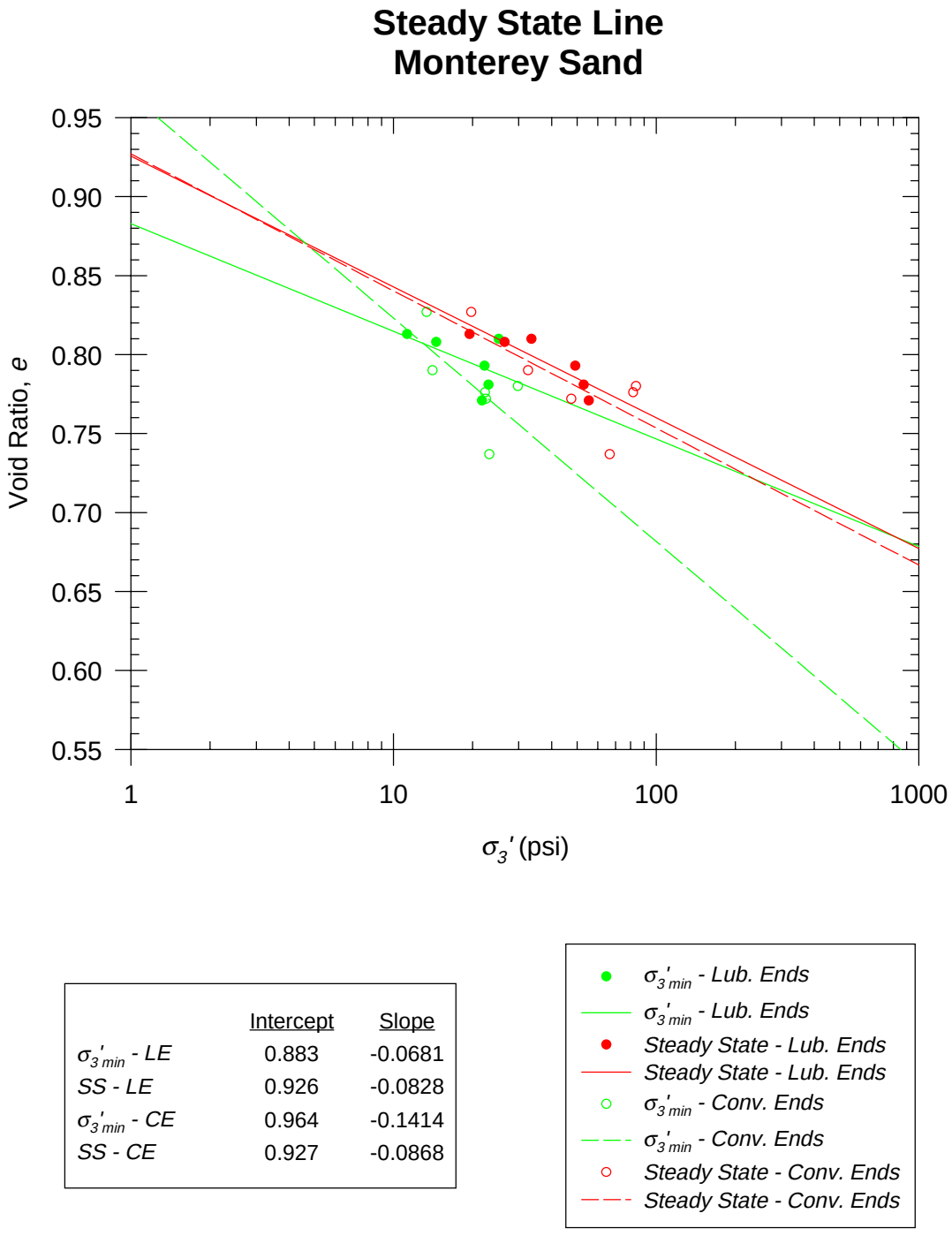

Figure 8.25 - Steady State Relationship for Monterey Sand

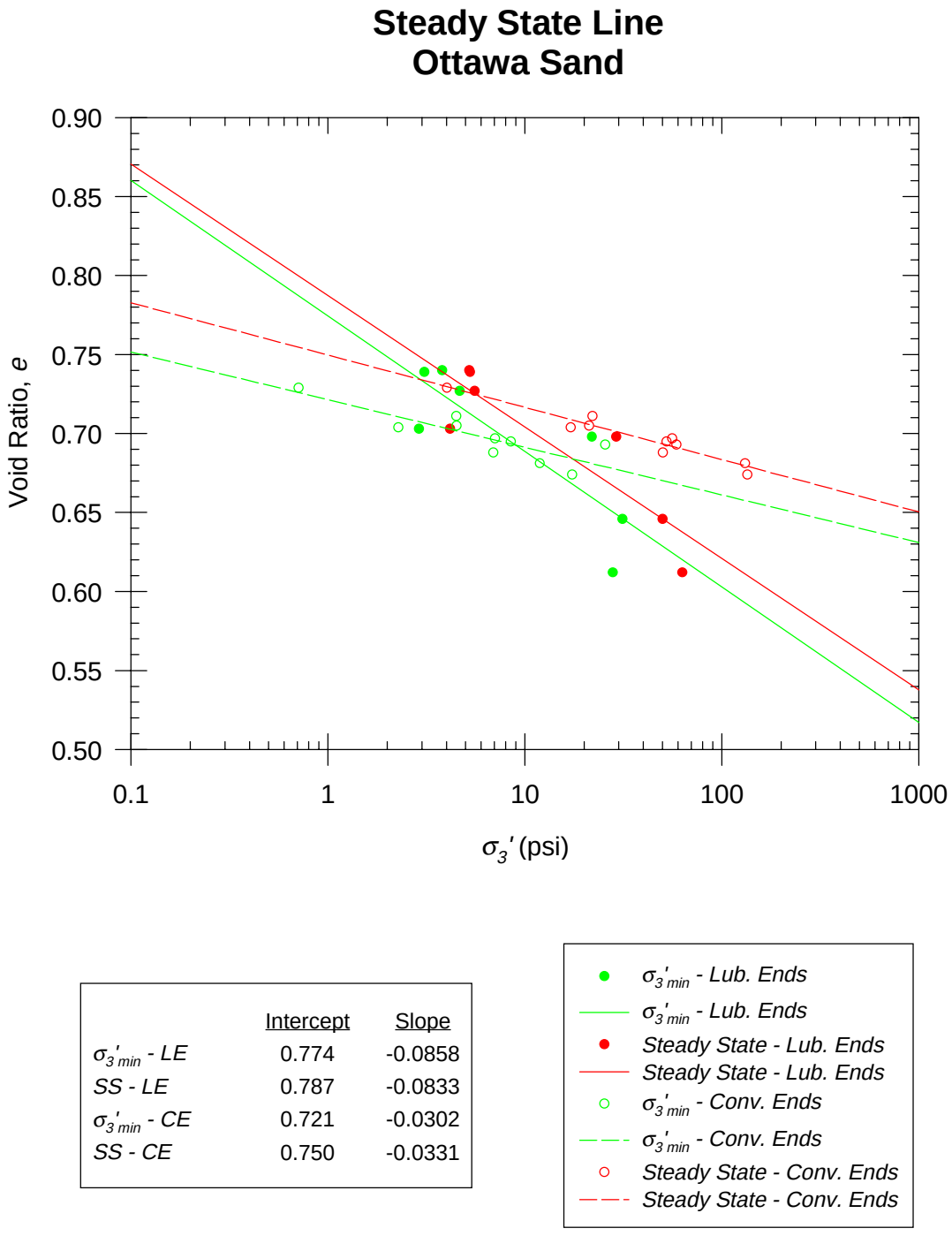

Figure 8.26 - Steady State Relationship for Ottawa Sand

Steady State Strength Envelopes

The steady state strength envelopes, based on the stress state variables p' and q, and the steady state friction angles associated with each condition are shown in Figure 8.27, Figure 8.28, and Figure 8.29. In general, much less scatter is observed in the strength envelopes than in the steady state lines. One reason for this is that the strength envelopes are not directly dependent on the void ratio, so errors in void ratio determination do not directly influence the strength envelopes. Also, as was shown in Figure 8.20, the end effects can significantly influence the stress conditions during shear at large strains, but the steady state friction angle may remain nearly constant as the stress path essentially follows the strength envelope. Figure 8.27, Figure 8.28, and Figure 8.29 demonstrate that for all tests, regardless of material, the minimum effective stress condition occurred at values of p' less than 60 psi, while the steady state condition occurred at values of p' as high as 230 psi. For the Light Castle sand, the steady state friction angle appears to be independent of both the type of end platens used and the condition that is used to define steady state conditions. The steady state friction angle for Monterey sand does not vary significantly with the type of end condition, but the values based on steady state are approximately 3° to 4° less than those based on the minimum effective stress condition. For the Ottawa sand, the steady state friction angle based on the minimum effective stress and using lubricated ends is very similar to that based on steady state using conventional ends. Likewise, the steady state friction angle based on the minimum effective stress and using conventional ends is very similar to that based on steady state using lubricated ends. No good rationale for this observed behavior has been proposed.

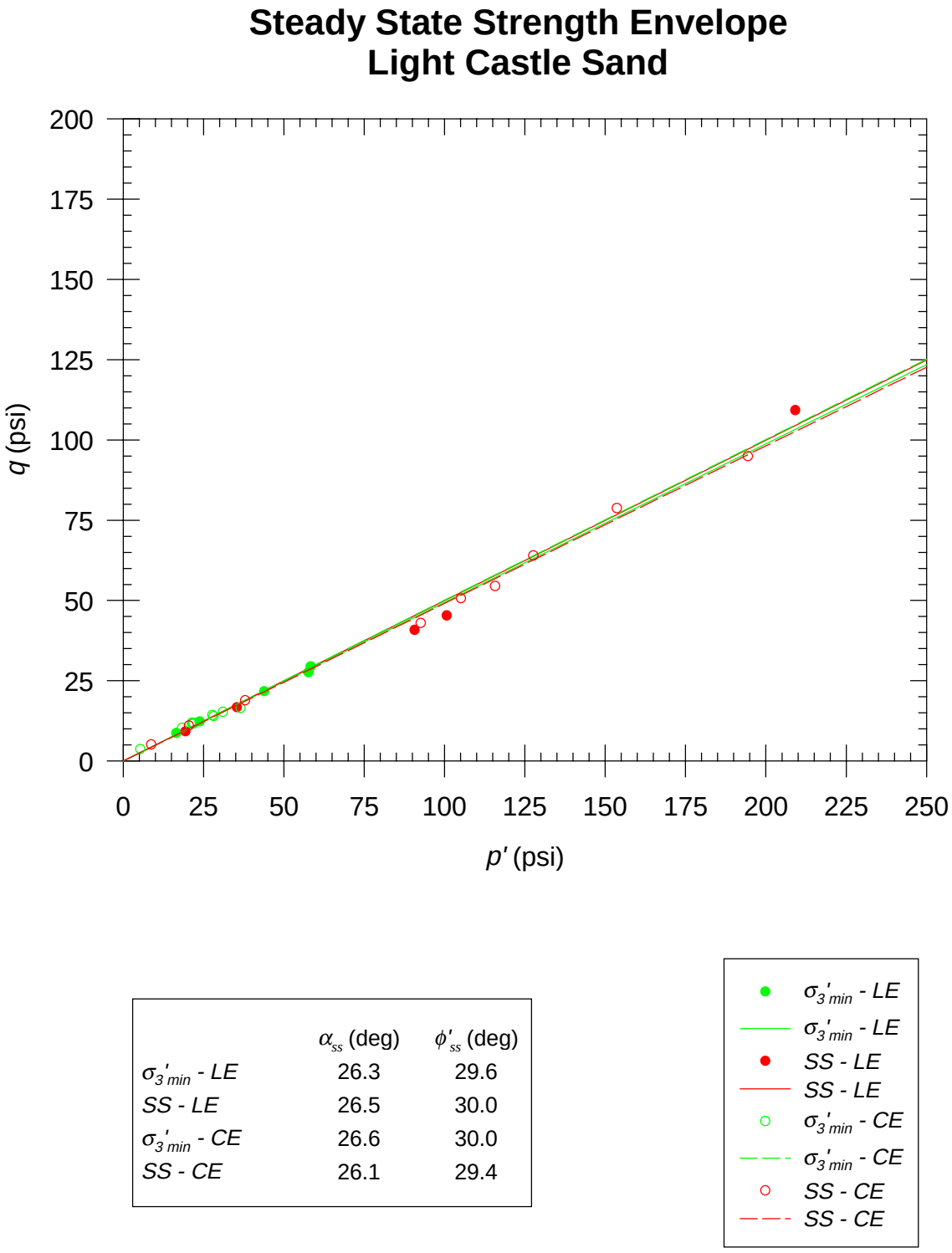

	α_{ss} (deg)	ϕ'_{ss} (deg)
$\sigma_{3'min}$ - LE	26.3	29.6
SS - LE	26.5	30.0
$\sigma_{3'min}$ - CE	26.6	30.0
SS - CE	26.1	29.4

Figure 8.27 - Steady State Envelope for Light Castle Sand

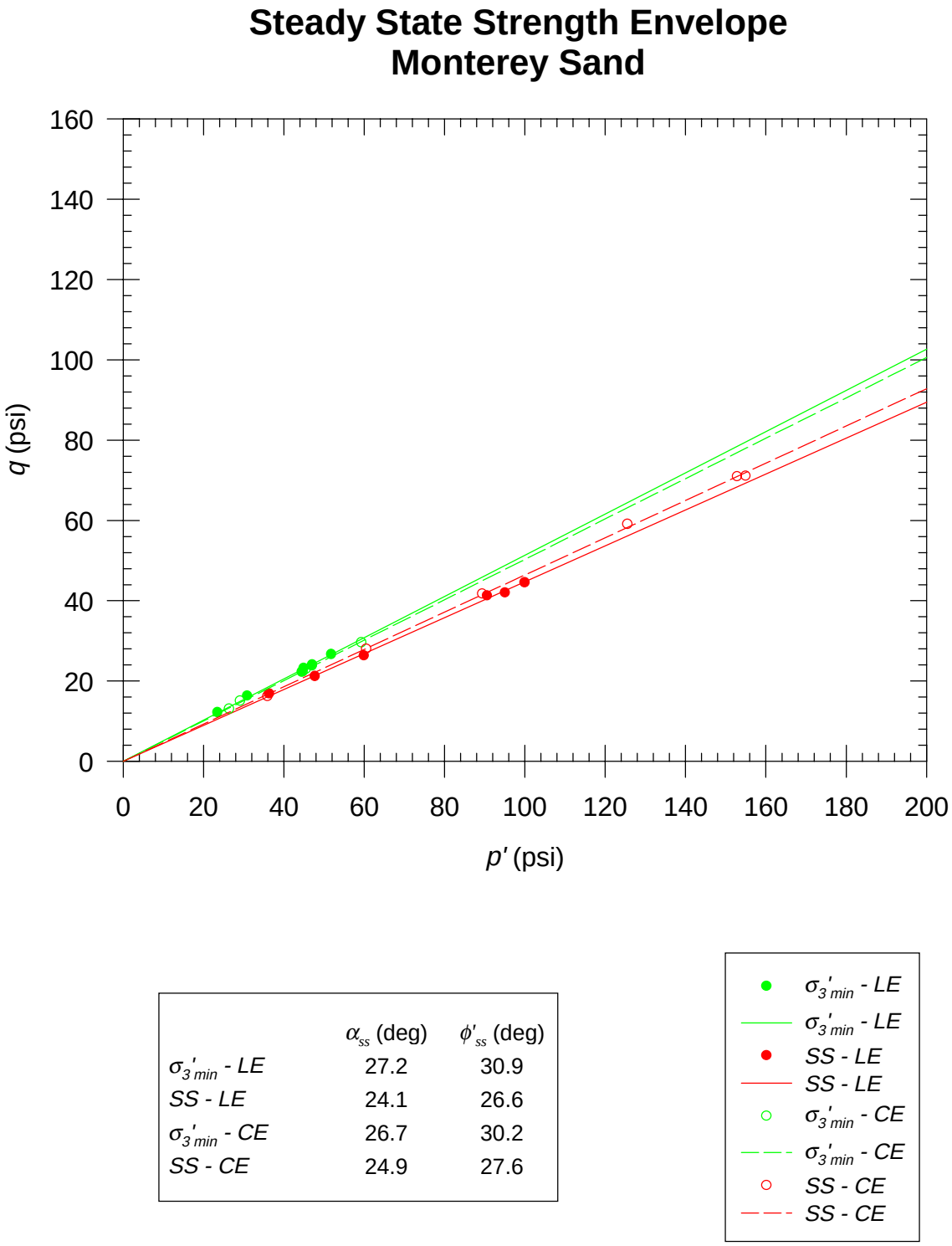

	α_{ss} (deg)	ϕ'_{ss} (deg)
$\sigma_{3'min}$ - LE	27.2	30.9
SS - LE	24.1	26.6
$\sigma_{3'min}$ - CE	26.7	30.2
SS - CE	24.9	27.6

Figure 8.28 - Steady State Envelope for Monterey Sand

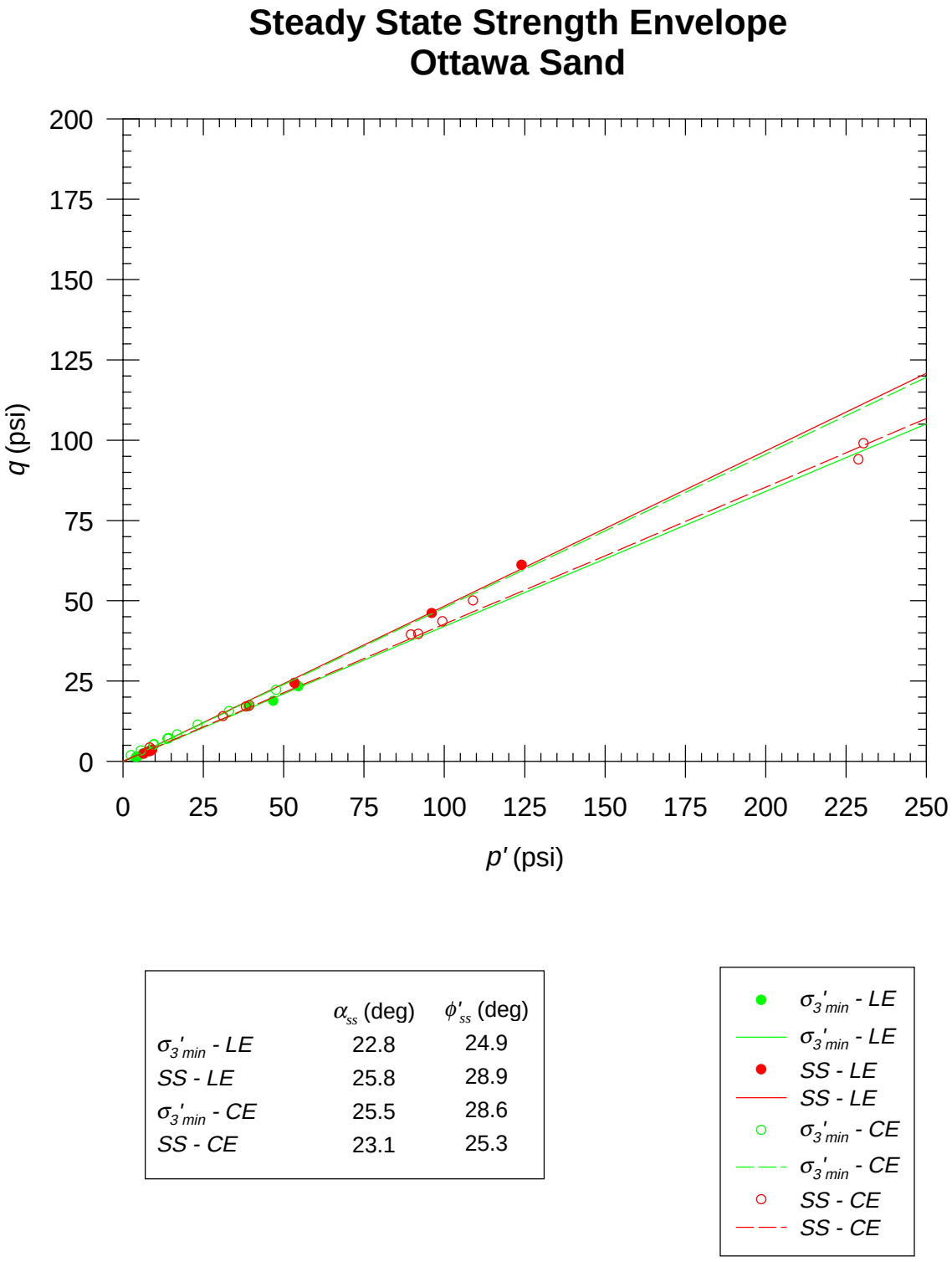

	α_{ss} (deg)	ϕ'_{ss} (deg)
$\sigma_{3'min}$ - LE	22.8	24.9
SS - LE	25.8	28.9
$\sigma_{3'min}$ - CE	25.5	28.6
SS - CE	23.1	25.3

Figure 8.29 - Steady State Envelope for Ottawa Sand

Summary

The influence of area corrections, membrane stress corrections, end friction effects, and membrane penetration effects on the data from the CU triaxial tests conducted as part of this research were evaluated. While the corrections applied to the data influence the derived steady state shear strength parameters, their influence does not appear to account for the scatter typically found in triaxial test data at large strain levels or steady state conditions. The area corrections have been shown to have a more profound impact on the calculated stresses than do the membrane corrections. For the membranes, soils, test conditions, and specimen geometry used in this study, the effect of applying the membrane corrections appears to be negligible. This does not imply that the influence of the membrane is negligible, but that the available methods for correcting for the stresses that develop in the membrane do not significantly alter the calculated stresses in the specimen.

The area correction applied, however, can significantly change the magnitude of the calculated stresses at various strain levels as well as to mask the true soil behavior. For example, the calculated stress based on the applied area correction may be varying with strain, while the actual deviator stress is constant.

The effects of end friction observed experimentally generally agree with those predicted analytically. Due to the complex behavior exhibited by granular materials during undrained triaxial tests, correcting for these effects is not practical. The experimental results indicate that end effects alone do not cause nonuniformity of test conditions, since nonuniform conditions eventually develop even in tests with lubricated end platens. The effects of end friction, however, do result in a tendency for nonuniform conditions to develop, and probably exacerbate the errors due to other inherent specimen variability

related to initial conditions, membrane effects, and nonuniform pore pressure development.

CHAPTER 9 CONCLUSIONS

The determination of the shear strength of soil that is subjected to monotonic, cyclic, or dynamic loads that result in significant straining of the soil is an important task for geotechnical engineers. The steady state approach has been used to describe the shear strength at large strains, but its accuracy has been questioned. This study was undertaken to examine the validity of determining steady state undrained shear strength, which typically requires large strain levels, using the conventional ICU triaxial test.

Summary of Work Accomplished

The concept of a steady state of deformation was described in the context of liquefaction susceptibility evaluation. Recommended procedures for determination of the steady state undrained shear strength and evaluation of liquefaction susceptibility based on this shear strength were reviewed. Various means of expressing the steady state relationship based on different stress state parameters were discussed.

The development of the triaxial test as a means for evaluating the shear strength of soils was briefly discussed. Recommended procedures for performing triaxial tests were described in detail. The various corrections that have been applied to triaxial test data were reviewed. The RCC area correction, central cylindrical bulging (partial RCC) correction, and the parabolic bulging correction for undrained loading have been described previously. The parabolic correction was extended to account for volume change during shear, and a sinusoidal correction was developed to describe another form of nonuniform deformation. Membrane strength corrections were reviewed, and an extended form of the membrane corrections for RCC deformation was proposed. These

corrections account for the combined axial and lateral loading of the membrane, but are based on Hooke's law and linear strain-displacement relations. An approximate correction for nonuniform deformation modes was derived from the correction for RCC deformation. Analytical and experimental studies of the effects of membrane penetration on test results were reviewed. The effect that membrane penetration can have on the measured steady state relationship was explicitly described.

Previous experimental studies of the effects of friction on the specimen ends were reviewed. Attempts to find analytical solutions to the completely restrained cylinder problem were discussed. Since analytical solutions only examined complete end restraint, finite element analyses were undertaken to evaluate the end effects for various degrees of end friction and for various elastic and elasto-plastic material models. In order to model varying degrees of end restraint, an axisymmetric, isoparametric interface element was developed and implemented.

Interface direct shear tests were performed in order to provide interface properties for the finite element analyses as well as to evaluate various candidate schemes for lubricating triaxial specimen-end platen interfaces. Tests were performed on seven different interfaces at varying values of normal stress.

ICU triaxial tests were performed on three different materials with both conventional and lubricated end platens. These tests were performed to experimentally investigate the influence that friction on the specimen ends has on ICU test results, as well as to provide data to evaluate the significance of the various corrections that can be applied to triaxial test data at large strain levels.

Conclusions

The conclusions with regard to corrections to triaxial test data can be summarized as follows:

1.) The area corrections to account for the changing specimen dimensions have a significant influence on the computed stress conditions within the specimen. This influence increases with increasing axial strain level. Since the true deformation mode of a specimen changes during a test carried to large strain levels, any analytical correction based on an assumed deformation mode is an estimate at best. Since nonuniform deformation occurs at large strains regardless of end conditions, the parabolic or sinusoidal corrections are most appropriate for tests conducted to determine steady state undrained shear strength.

2.) The corrections to account for the stresses in the membrane are much less significant than those to account for area changes. Again, the corrections are an estimate since they are based an assumed mode of deformation. The correction to the lateral stress has been shown to be negligible for tests in which volume change is prevented (saturated undrained conditions), even at large values of axial strain. The correction to the axial stress can be important, particularly for weak specimens at large strains, so it should be applied to tests performed to determine steady state undrained shear strength.

3.) The effects of membrane penetration and compliance on steady state relationships may be more significant than previously thought. Accounting for volume changes due to membrane penetration has been shown to flatten the steady state line, making the relationship even more sensitive to void ratio. Furthermore, previous studies have shown that membrane compliance can reduce the tendency for pore pressure development by as

much as 50 percent. If this reduction in pore pressure development occurs in tests used to determine the steady state line, the true slope of the line should be even flatter still.

The conclusions with regard to the effect of friction on the specimen ends on triaxial test data can be summarized as follows:

1.) The effects of end friction on triaxial test specimens can be adequately modeled using the finite element method and axisymmetric isoparametric interface elements. Axisymmetric interface elements should be integrated using Gauss quadrature rather than Newton-Cotes integration since numerical problems can arise using the latter.

2.) Results of finite element analyses indicate that the friction on the specimen ends stiffens the apparent stress-strain relationship, or increases the measured modulus. The distribution of stresses in the specimen is nonuniform due to the friction imposed on the ends. The nonuniform stress distributions result in a progressive failure within the specimen, rather than failure of the entire specimen at a single value of applied axial load.

3.) The influence of the end friction is apparent even for a linearly elastic material, but has more influence on measured properties after failure for an elasto-plastic material.

4.) The effects of end friction based on interface characteristics of conventional end platens are much less significant than those based on complete restraint. For the material models used in this study, the end effects are minimal when interface characteristics of lubricated end platens are modeled.

The conclusions with regard to interface direct shear tests can be summarized as follows:

1.) The behavior of typical end platen-specimen interfaces can be evaluated experimentally using a modified direct shear test. The behavior can be modeled analytically using a bilinear stress-strain relationship, although the initial response is slightly curved. The initial shear stiffness is related to the normal stress on the interface. The shear stiffness after failure is essentially zero.

2.) For typical interfaces between conventional end platens and sand specimens, the value of the interface friction angle is approximately 29 degrees.

3.) For typical interfaces between lubricated end platens and sand specimens, a value of the interface friction angle less than 1 degree can be achieved.

4.) For lubricated end tests on sand specimens, the lubrication scheme using Teflon tape, steel shim material, and vacuum grease provides better shear lubrication than the more popular scheme using thin latex and vacuum grease. The better performance is due to the fact that stress concentrations between individual sand grains and the end platen are prevented.

In the triaxial test, the following factors limit the usefulness of the results when determining the steady state undrained shear strength:

1.) No matter which method of specimen preparation is employed, a perfectly uniform specimen cannot be fabricated. Inherent variations within the specimen prior to testing may affect both the consolidation response under an increase in effective confining stress and the stress-

strain response of the specimen during shear. Although the steady state of deformation, by definition, requires that enough shear strain has occurred such that any initial fabric or structure has been destroyed, the variations in specimen density or fabric may amplify the errors due to other problems that occur during shear, such as the influence of the end platens on the stress and strain distributions within the specimen or the density variations as a result of pore fluid migration within the specimen.

2.) The influence of rigid end platens with highly frictional surfaces has a significant impact on the stress and strain distributions within the specimen, even for a length to diameter ratio of 2. Nonuniform distributions will occur in an ideal homogeneous, isotropic material. Their significance may increase in sand specimens with initial nonuniformities. Although a relatively uniform distribution of stress and strain can be maintained through a larger range of axial strains with lubricated end platens than with conventional end platens, nonuniformity of stress and strain will eventually occur.

3.) The length of the drainage path and rate and duration of loading in an undrained triaxial test may be quite different than those that occur in the field. The *in situ* soil experiences undrained shear because these conditions prevent drainage and dissipation of pore pressures that develop as a result of the applied load. In the undrained triaxial test, drainage is prevented across the specimen boundaries and a constant specimen volume is maintained. In order to accurately measure pore pressures, the strain rate is typically slow enough to allow for equalization of pore pressure gradients that have been shown to develop within the specimen, particularly at large strains. This equalization is accompanied by pore fluid migration and variations in density on a local basis and inherently results in some nonuniformity of the test specimen.

Since undrained loading in the field is typically a result of rate effects rather than fixed boundary conditions, an *in situ* soil deposit may respond to a particular load quite differently than the test specimen, especially at large strain levels that are typically associated with steady state conditions.

In using the steady state procedure for liquefaction susceptibility evaluation, it is imperative that an accurate description of the steady state strength versus void ratio relationship be obtained. The CU triaxial test has been a popular means of measuring this relationship. If the relationship measured in the triaxial test is to be reliable, the actual stress and density conditions in the soil that is undergoing steady state deformation must be measured. In the triaxial test, average conditions of the entire specimen are typically measured. If the test is performed such that the stress and density distributions within the specimen are uniform, then the entire specimen should undergo a steady state of deformation simultaneously, and the average values should be accurate. If, however, all regions of the specimen do not achieve steady state conditions simultaneously, then the average values of stress and density for the entire specimen will be in error. It can be shown experimentally that reasonably uniform stress and density distributions can be maintained over larger ranges of strain if careful specimen preparation techniques, careful test procedures, and lubricated end platens are used. However, at strain levels much greater than those required for failure, nonuniform stress and density distributions almost always develop. Since large, post-failure strain levels are usually required to reach steady state conditions, the steady state relationship based on measured average values will be in question.

The concept of steady state deformation provides valuable insight into the fundamental behavior of cohesionless soils when shear strain levels far exceed those required for failure. It provides a rational basis for understanding the

difference in behavior of loose and dense soils in response to both drained and undrained loading. However, it's value as a means of evaluating liquefaction susceptibility *when the steady state undrained shear strength is based on CU triaxial tests* appears to be limited. Other types of laboratory tests may provide a more accurate description of the stress state and density at large strains, and hence improve the accuracy of the steady state relationship. It seems that with due care it is possible to reach steady state conditions in the triaxial test while maintaining a fairly accurate record of the stress state. However, this occurrence is not guaranteed, despite careful specimen preparation and test procedures. The influence of testing errors and corrections to account for those errors have been demonstrated, but can not wholly account for the variation in the measured steady state undrained shear strength. Likewise, the effects of friction on the specimen ends contributes to the nonuniform conditions that develop, but cannot explain the variation in measured strengths as well.

Recommendations for Further Research

The accurate determination of the steady state relationship requires knowledge of both the stress conditions and the volumetric conditions at large axial strain levels. An analytical procedure for correcting the measured average values in order to estimate the stresses in a local region undergoing steady state deformation might be possible, but the extreme sensitivity of the steady state relationship to void ratio suggests that this technique would be no better than using the average values for the entire specimen. However, further analytical studies based on true effective stress constitutive models and couple the stress-displacement behavior and flow of pore fluid within the sample may provide valuable insight into the extent that nonuniform density develops and its influence on measured properties. A better understanding of the nonuniform conditions that develop as large shear strains occur may allow

specific improvements to testing procedures or equipment to help minimize the variations that contribute to measurement errors. If the nonuniform conditions cannot be prevented, then procedures to measure the density and stress states in a local region within a specimen may make a much more accurate determination of the steady state relationship possible. Some promising techniques for the measurement of specimen density using electromagnetic radiation are being investigated (Finno et al. 1996, Frost and Kuo 1996), and may prove invaluable in determining the conditions in localized regions of soil specimens. Presently, this technology is still immature, but its impact on the accurate measurement of specimen properties at large strains could be significant. If the accuracy of the steady state approach based on CU triaxial test data is to be improved, improved methods and new technology for accurately determining either the stress conditions or the volumetric conditions on a local basis will be required.